Virginia Commonwealth University

VCU Scholars Compass

2023

CHARACTERIZING THE EFFECTS OF ANTIANDROGENS AND SENOLYTICS TO ENHANCE THE THERAPEUTIC RESPONSE TO CASTRATION-RESISTANT PROSTATE CANCER

Justin M. Silverman
Virginia Commonwealth University

CHARACTERIZING THE EFFECTS OF ANTIANDROGENS AND SENOLYTICS TO ENHANCE THE THERAPEUTIC RESPONSE TO CASTRATION-RESISTANT PROSTATE CANCER

A dissertation submitted in partial fulfillment of the requirements for the degree of Master of Science at Virginia Commonwealth University.

By

Justin Maurice Silverman

Virginia Commonwealth University

Advisor: David A. Gewirtz, PhD

Professor, Department of Pharmacology & Toxicology

School of Medicine

Virginia Commonwealth University

Richmond, VA

July 2023

Acknowledgments

If you had asked me three years ago where I would be today, I wouldn't have said completing my master's degree. Three years ago, I was working at a law firm as a patent assistant and did not know what I wanted. Now, I've wrapped up the most significant accomplishment of my life so far and I am about to embark on an even more profound journey by starting my Ph.D. While I'm proud of who I've chosen to become as a person and where I am today, I wouldn't have gotten to this point without the support of my friends and family, especially my parents. They've always supported my goals and dreams no matter what and I am very grateful to have them in my life. Of course, I also must acknowledge and thank Dr. David Gewirtz, who's been such a supportive mentor and I certainly couldn't have done any of this without him. I would also like to thank Valerie De Luca who trained me when I first arrived as well as my current and former lab mates Ahmed, Melanie, Eesha, Marissa, Rana, Ryan, Fereshteh and Muruj. Finally, I would like to thank my committee members, Drs. Damaj and Reed, as well as the Pharmacology and Toxicology Department.

Table of Contents

Abbreviations

AA   Abiraterone Acetate

ACTH   Adrenocorticotropic Hormone

ADT   Androgen Deprivation Therapy

AR   Androgen Receptor

ATG   Autophagy-related gene or protein

Bad   BCL2 associated agonist of cell death

Bak   Bcl-2 Homologous Killer

Bax   Bcl-2-Associated X Protein

BCL-2   B-Cell Lymphoma 2

BCL-W   Bcl-2-Like Protein 2

BCL-XL   B-Cell Lymphoma-Extra Large

BET   Bromo- and Extra-Terminal Domain

BH3   BCL-2 Homology Domain 3

BIM   Bcl-2 Interacting Mediator of cell death

BRD 2/3/4   Bromodomain-Containing Protein 2/3/4

BSA   Bovine Serum Albumin

C12FDG   5-Dodecanoylaminofluorescein Di-β-D-Galactopyranoside

CDK   Cyclin-Dependent Kinase

CMA   Chaperone-Mediated Autophagy

CRPC   Castration-Resistant Prostate Cancer

CS   Charcoal-Stripped

CYP   Cytochrome P

DMEM   Dulbecco's Modified Eagle Medium

DNA   Deoxyribonucleic acid

Doc   Docetaxel

Enza   Enzalutamide

FACS   Fluorescence-Activated Cell Sorting

FBS   Fetal Bovine Serum

GAPDH   Glyceraldehyde 3-Phosphate Dehydrogenase

HSLCI   High Speed Live Cell Interferometry

IC-50   Half Maximal Inhibitory Concentration

LC3 I/II   Light Chain Microtubule-Associated Protein

MCL-1   Myeloid Cell Leukemia-1

mCRPC   Metastatic Castration-Resistant Prostate Cancer

nmCRPC   Nonmetastatic Castration-Resistant Prostate Cancer

NSAA   Nonsteroidal Antiandrogens

NSCLC   Non-Small Cell Lung Cancer

OS   Overall Survival

PARP   Poly ADP Ribose Polymerase

PBS   Phosphate Buffered Solution

PCa   Prostate Cancer

PI   Propidium Iodide

PROTAC   Proteolysis-Targeting Chimera

PSA   Prostate-Specific Antigen

Rb   Retinoblastoma protein

RNA   Ribonucleic acid

RPMI   Roswell Park Memorial Institute

SA-β-Gal   Senescence-Associated-β-Galactosidase

SAHF   Senescence-Associated Heterochromatic Foci

SASP   Senescence-Associated Secretory Phenotype

SEM   Standard Error of the Mean

TIS   Therapy-Induced Senescence

XRA   Radiation Therapy

Abstract

Prostate cancer is the most frequently diagnosed cancer in males and the second most common cause of cancer deaths. Androgen deprivation therapy, whether through surgical or chemical castration, is the mainstay for treatment of advanced prostate cancer; however, despite an initial response, most patients eventually develop a progressive PSA rise, and castration-sensitive prostate cancer gives rise to castration-resistant prostate cancer. The standard of care therapy includes the antiandrogens such as enzalutamide and abiraterone acetate as well as the microtubule poison, docetaxel, and various immunotherapies; however, while prostate cancer research is progressing, there continues to be a compelling need for new and more efficacious treatment combinations to prolong survival and offset disease progression, especially for castration-resistant disease.

While the role of antiandrogens in androgen-dependent prostate cancer is well characterized, this is not the case for the involvement of these therapies in androgen-independent disease. Furthermore, successful utilization of senolytics to target senescent cells in cancer treatment has not yet been implemented or approved for clinical use.

Initially, we evaluated the standard of care anti-androgens, enzalutamide and abiraterone, and their ability to induce growth arrest and possibly senescence in the PC3 and DU145 androgen-independent cell lines. While treatment with these antiandrogens produced a transient, growth arrest response, even in the case of supraclinical concentrations, neither drug induced significant senescence in either cell line. Despite these initially negative results, this did not rule out the possibility that a potential senolytic such as the BET degrader, ARV-825, could enhance the response to antiandrogens; therefore, we hypothesized that ARV-825 could potentially improve androgen independent castration-resistant prostate cancer's response to enzalutamide.

While the ARV-825 failed to enhance the response to enzalutamide in combination in PC3 cells, it had a significant effect as a monotherapy. Additional studies to understand the ineffectiveness of ARV-825 in the combination proved to be challenging, with enzalutamide inducing protective autophagy being a possible explanation. The most promising direction derived from these studies is the possible use of ARV-825 as a monotherapy in androgen-independent disease. ARV-825 as a monotherapy induced a significant prolonged growth arrest in the androgen-independent cells along with decreased levels of BRD4 and c-Myc. However, the ARV-825 did not induce significant senescence or apoptosis, despite the substantial growth arrest; therefore, the nature of this growth arrest remains to be investigated. Nevertheless, ARV-825 could prove to be a clinically relevant strategy in the treatment of castration-resistant prostate cancer.

Chapter 1: General Introduction

1.1. Prostate Cancer

1.1.1. Prostate Cancer Overview

Prostate cancer (PCa) is the most frequently diagnosed cancer in males and the second most common cause of cancer deaths [1]. In the U.S., it is estimated that about 34,000 men die from prostate cancer each year [2]. Globally, prostate cancer is the most diagnosed malignancy with more than 1.4 million men newly diagnosed in 2020 [3].

The diagnosis and classification of prostate cancer can be placed into context within a series of clinical states. These states begin with localized disease, followed by the locally advanced rising prostate-specific antigen (PSA) state and the advanced metastatic state. Finally, there are the castration-resistant states, which for most men are lethal within a few years [4]. Androgen deprivation therapy (ADT), whether through surgical or chemical castration, is the mainstay for treatment of advanced PCa; however, despite initial response, most patients eventually develop a progressive PSA rise, and castration-sensitive prostate cancer gives rise to castration-resistant prostate cancer (CRPC) [5]. The term "castration resistant" is preferred over the previously used designations of "androgen independent" and "hormone refractory" disease because, despite the absence of circulating testosterone, the tumor remains functionally dependent on androgens and on the androgen receptor, though the disease can eventually progress to being entirely "androgen independent" [6]. The development of resistance has been attributed to several mechanisms, spanning from those associated with androgen receptor signaling to novel pathways acting independently of the androgen axis, such as those involving

RAS/MAP kinase, transforming growth factor-beta/SMAD pathway, fibroblast growth factor signaling, JAK/STAT pathway, Wnt-Beta catenin, and hedgehog signaling [7]–[9].

1.1.2. Standard of care treatments for CRPC and their mechanisms of action

While localized disease can be treated with a combination of surgery, radiation, and ADT, once the disease progresses to CRPC, the treatment regimen changes significantly [10]. When it comes to CRPC, the disease can be nonmetastatic (nmCRPC) or metastatic (mCRPC). Nonmetastatic CRPC tends to be less fatal than metastatic CRPC and there are only three drugs used in its treatment in conjunction with castration. These are the anti-androgens apalutamide, darolutamide and enzalutamide with apalutamide being the first medication approved to specifically treat nmCRPC [11]. All three of these drugs are second generation nonsteroidal antiandrogens (NSAAs) that act as selective competitive silent antagonists of the androgen receptor (AR), via the ligand-binding domain with varying levels of activity and distribution [12].

Metastatic CRPC, on the other hand, has a variety of 1st line and 2nd line treatments including the antiandrogen, enzalutamide. Docetaxel, a microtubule inhibitor and the first systemic therapy to demonstrate survival benefit in mCRPC, was studied in two prospective phase III trials [13], [14]. In both studies, docetaxel administered every three weeks demonstrated a survival benefit, with a median overall survival (OS) gain of (a relatively modest) 1.9 to 2.4 months, establishing docetaxel as the new standard of care for mCRPC in 2004. Docetaxel is believed to have a twofold mechanism of antineoplastic activity: (1) inhibition of microtubular depolymerization, and (2) attenuation of the effects of Bcl-2 and Bcl-xL anti-apoptotic gene expression that ultimately leads to apoptotic cell death [15]. Cabazitaxel

is a tubulin-binding drug with demonstrated activity in docetaxel-resistant cancers, and is thus a 2nd line treatment [16]. Abiraterone acetate is a selective inhibitor of cytochrome P (CYP) 17, a key enzyme in androgen synthesis [17]. Early in the development of abiraterone acetate, research showed that inhibition of CYP17 could increase adrenocorticotropic hormone (ACTH) levels up to sixfold. Elevated ACTH can result in mineralocorticoid excess, which can be countered with corticosteroids [18]. Compared to prednisone alone, the combination of abiraterone acetate and prednisone in both the pre- and post-docetaxel settings demonstrated superior gains in all clinical measures, including time to initiation of cytotoxic chemotherapy, opiate use for cancer-related pain, PSA progression, decline in performance status, and overall survival [19], [20]. Enzalutamide, mentioned previously, binds competitively to the ligand-binding domain of the androgen receptor and inhibits androgen receptor translocation to the cell nucleus and androgen receptor binding to DNA [21]. Patients who received enzalutamide had higher median OS (18.4 versus 13.6 months), with a 37% decrease in risk of death [22].

Other treatments include radioisotopes such as samarium-153 and strontium-89, which have long been a therapeutic option, either as monotherapy or in combination with chemotherapy, in the management of advanced prostate cancer; however, these isotopes are beta emitters with potential to cause bone marrow toxicity [23], [24]. Radium-223, on the other hand, is an alpha-emitting calcium mimetic that binds to the microenvironment of metastases with a considerably narrower range of irradiation compared with beta emitters and, therefore, lower risk of hematologic complications [25]. There has also been success with the autologous cellular immunotherapy, Sipuleucel-T, which is approved for treatment of asymptomatic or minimally symptomatic mCRPC. It is composed of autologous antigen-presenting cells cultured with a fusion protein, PA2024, which consists of prostatic acid phosphatase linked to granulocyte-

macrophage colony-stimulating factor [26]. Furthermore, poly(ADP–ribose) polymerase (PARP) inhibition has long been explored as a therapeutic strategy for breast and ovarian cancers, especially in cases with underlying *BRCA1/2* or other germline DNA damage repair defects. Large-scale multicenter efforts recently demonstrated germline defects in DNA damage repair genes in up to 11.8% of men with advanced prostate cancer [27]. As a result of recent successful trials, the FDA granted breakthrough designation for olaparib in mCRPC to accelerate its development [28]. Finally, research into the immune checkpoint inhibitors, despite their practice-changing clinical outcomes in other solid tumors, have yet to demonstrate efficacy in prostate cancer. More recently, pembrolizumab showed a high response rate in tumors with mismatch repair deficiency, regardless of primary site, leading to a tissue-agnostic FDA approval [29]. With some studies suggesting that 2–12% of prostate cancers harbor microsatellite instability and a hypermutated state, pembrolizumab represents a new therapeutic option for a subset of mCRPC [30], [31]. Given the variety of treatment options becoming available for men with mCRPC, prostate cancer research is progressing in the right direction; however, particularly with respect to the development of castration resistant disease, there continues to be a compelling need for new efficacious treatment combinations to prolong survival and offset disease progression.

1.2. Senescence

1.2.1 Senescence Overview

Our understanding of cellular senescence, a specialized form of stable growth arrest initially described by Leonard Hayflick in the 1960s, has evolved dramatically through the decades [32]. Irreversibility was long considered a critical characteristic that distinguished senescence from other forms of growth arrest such as quiescence, a transient form of growth

arrest; however, over the past few decades, hallmarks of senescence have been identified that collectively characterize a more complex, unique phenotype [33], [34]. Several biological contributions of cellular senescence in homeostatic and pathological processes have also been identified [35]. The induction of senescence in response to telomere shortening occurring because of successive cell duplication is not only an indicator of cellular mortality and aging but represents a fundamental tumor-suppressor mechanism [36], [37]. That is, the stability of senescent growth arrest is a barrier against the progression of genetically unstable cells that carry a dangerous malignant potential, which accounts for the accumulation of senescent cells in premalignant lesions [38]. This tumor-suppressive trait of senescence is also related to its role as a stress response to noxious stimuli such as oxidative stress, which partially explains the increased burden of senescent cells in aging organisms [39]. Cancer cells, therefore, can undergo senescence in response to severe stress induced by the exposure to a wide variety of cancer therapeutics, often termed, Therapy-Induced Senescence (TIS) [40].

In addition to the stable form of growth arrest that is a primary characteristic of senescence, senescent cells display a variety of qualities that together represent this senescent phenotype [41] (**Figure 1.1**). Fundamentally, senescent cells are characterized by flattened and enlarged morphology. They exhibit several molecular markers, including telomere-dysfunction-induced foci, senescence-associated heterochromatin foci (SAHF), lipofuscin granules, DNA scars, and altered gene expression [42], [43]. Another essential feature defining senescent cells is the production of a diverse range of cytokines, chemokines, extracellular matrix proteases, growth factors, and other signaling molecules, collectively termed the senescence-associated secretory phenotype (SASP), which largely mediates the extrinsic effects of senescence [44]. Furthermore, these cells can exhibit special biochemical characteristics, including the absence of

proliferative Ki-67 protein, enhanced activity of senescence-associated β-galactosidase (SA-β-gal), and expression of tumor suppressors and cell cycle inhibitors [43], [45]. Given that some of these features are not uniquely specific to senescence, senescent cells are usually identified by the examination of a profile of multiple senescence-associated biomarkers [46].
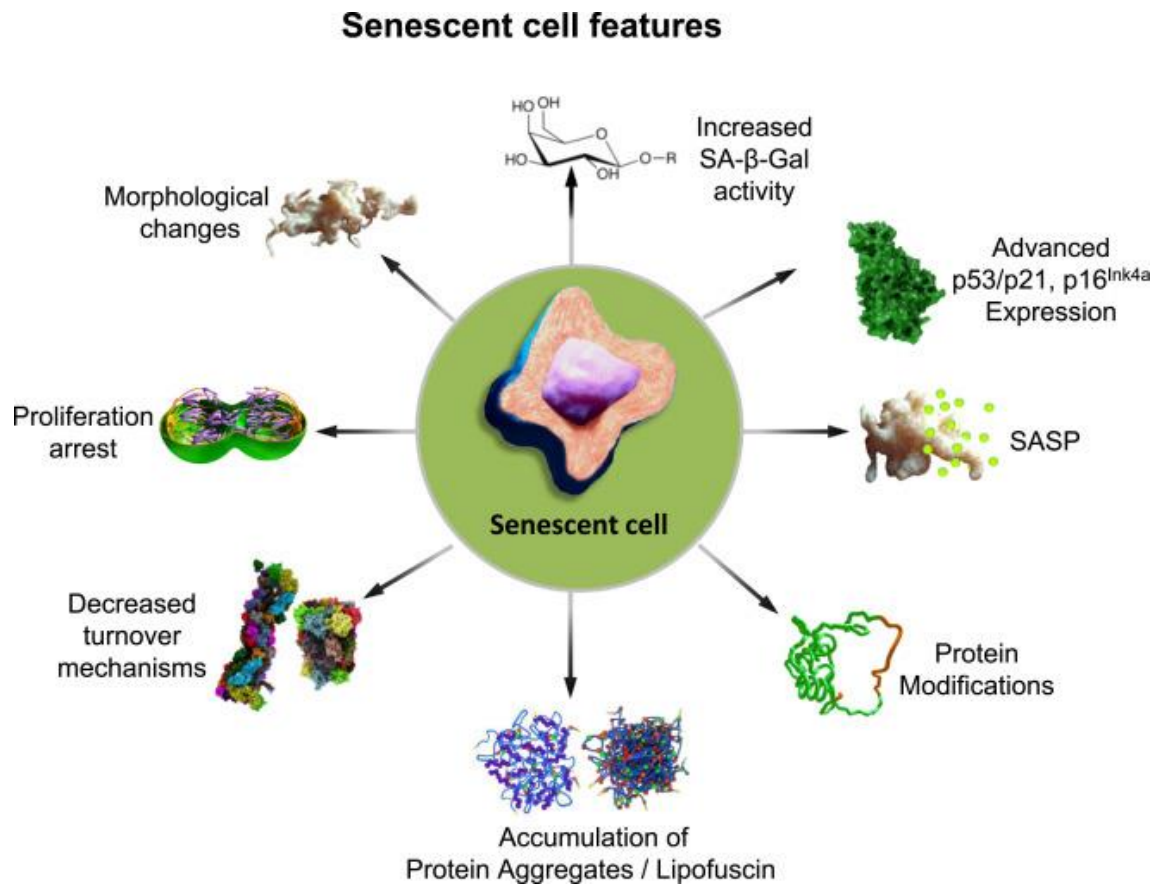
Figure 1.1 The features of senescent cells. Several markers were identified to characterize the senescent state in relation to morphology and proteostasis [160].

1.2.2. Senescence-targeted therapies

Studies building upon the phenomenon of replicative senescence in normal cells approaching the limit of their reproductive potential have identified a comparable senescence-

like arrest as a component of the traditional tumor cell response to chemotherapeutic drugs and radiation, which has been termed "premature senescence" or "accelerated senescence" [47]. While senescence has been seen as an ideal tumor cell response in the past, recovery from senescence could contribute to disease recurrence, and is often associated with the development of more aggressive and drug-resistant phenotypes [48]. Nevertheless, recent data has shown that the selective removal of senescent cells can delay or eliminate the recurrence of cancer; senolytics, senostatics and senomorphics are novel, small molecules that can target these senescent cells [49]–[51].

Senolytics are drugs that selectively eliminate senescent cells by targeting proteins involved in pro-survival and anti-apoptotic mechanisms such as the Bcl-2 family proteins [52]. In contrast to senolytics, senostatics do not kill senescent cells but inhibit paracrine signaling and thus block the 'proliferation' of senescence due to the bystander effect; studies have shown antioxidants or inhibitors of NF-κB can be efficient senostatics, with many others showing evidence as well [53]. Meanwhile, senomorphics suppress the detrimental effects of SASP components secreted by senescent cells without causing cell death. The first senomorphics were mainly discovered by serendipity including rapamycin, metformin, resveratrol and aspirin [54]. Our lab has demonstrated success using the senolytic ABT-263 for the clearance of TIS cells by interfering with the BCL-XL and BAX interaction in various cancer models [49], [55], [56]. ABT-263, or navitoclax, is a known BH3 mimetic drug and potently binds to the BH3 domain of BCL-2 anti-apoptotic members [57]. Upon administration, navitoclax binds to the BH3 binding groove of BCL-2 proteins which are located in the cytoplasm, causing the displacement of pro-apoptotic BH3-only protein, BIM, from BCL-2 [58]. BIM is then set free to trigger the release of small heme proteins, the cytochrome c, from mitochondria causing cell apoptosis [58].
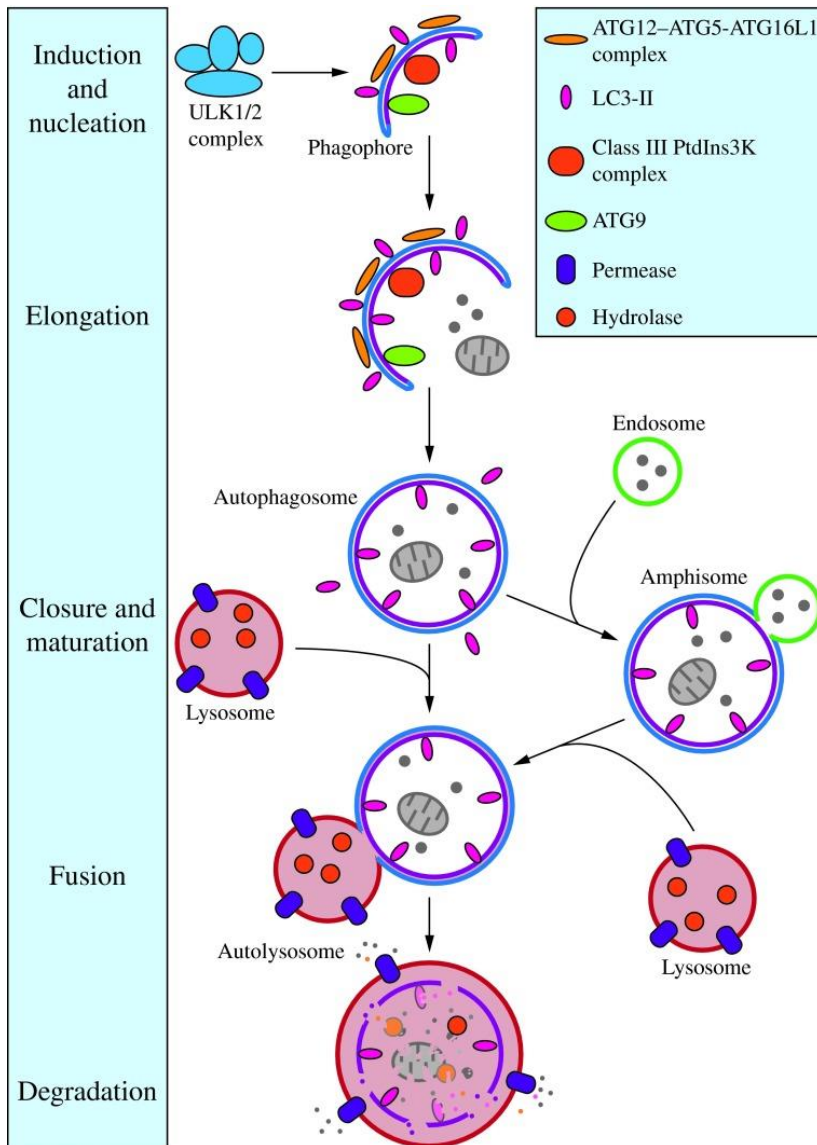
1.3. Autophagy

1.3.1. Autophagy and its mechanism

Autophagy is a highly conserved eukaryotic cellular recycling process. Through the degradation of cytoplasmic organelles, proteins, and macromolecules, and the recycling of the breakdown products, autophagy plays important roles in cell survival and maintenance [59]. In mammalian cells, there are three primary types of autophagy: microautophagy, macroautophagy, and chaperone-mediated autophagy (CMA). While each is morphologically distinct, all three culminate in the delivery of cargo to the lysosome for degradation and recycling [60]. During microautophagy, invaginations or protrusions of the lysosomal membrane are used to capture cargo [61]. Uptake occurs directly at the limiting membrane of the lysosome, and can include intact organelles. CMA differs from microautophagy in that it does not use membranous structures to sequester cargo, but instead uses chaperones to identify cargo proteins that contain a particular pentapeptide motif; these substrates are then unfolded and translocated individually directly across the lysosomal membrane [62]. In contrast to microautophagy and CMA, macroautophagy involves sequestration of the cargo away from the lysosome. In this case, *de novo* synthesis of double-membrane vesicles—autophagosomes—is used to sequester cargo and subsequently transport it to the lysosome [63]. Macroautophagy is the autophagic pathway that is most frequently implicated in cancer cell resistance to therapy, including hormonal therapy resistance [64].

Activation of autophagy is regulated by several stress factors, including hypoxia, nutrient starvation, ATP/AMP levels, ROS and microbial infection [65]. During the macroautophagic process, a double-membrane vacuolar compartment is formed, the vacuoles fuse with lysosome and the degraded contents are released into the cytosol (**Figure 1.2**). Under normal conditions,

mammalian target of rapamycin (mTOR) complex 1 negatively regulates autophagy by phosphorylating and binding to Unc-51 like autophagy activating kinase 1 (ULK-1), thus inactivating ULK-1 [66]. Under conditions of cellular stress, ULK-1 becomes dephosphorylated and dissociates from mTOR [66]. Initiation of autophagy occurs through the activation of the ULK-1 complex, which triggers the nucleation of the phagophore through phosphorylation of PI3KC3, VPS34 and Beclin-1 [67]. This preautophagosomal structure is hypothesized to come from multiple sources, such as the endoplasmic reticulum, mitochondria, Golgi apparatus, and recycling endosomes [68]–[71]. Following this initiation step, the phagophore is further elongated by the recruitment of autophagy regulatory proteins (ATG), such as ATG5 and ATG7 [72]. Microtubule-associated protein light chain 2 (MAP1-LC3) is lipidated by ATG3-mediated conjugation and incorporated into the growing phagophore, and is necessary for the closure, fusion and maturation of the autophagosome [73], [74]. Cargo is sequestered into the autophagosome by SQSTM1/p62, a sequestosome that binds ubiquitinated proteins and anchors itself to LC3 located on the inner membrane of the autophagosome [73]. The growing phagophore extends until the two ends join and fuse together to form a double-membrane vesicle, or the autophagosome [72]. In the final step, the mature autophagosome fuses with the lysosome to form the autolysosome. The acidic hydrolases of the lysosome then degrade the cargo within the autophagosome, which is then released into the cytoplasm for cellular repurposing [75]. At the same time, LC3-II in autolysosomal lumen is degraded. Thus, lysosomal turnover of the autophagosomal marker LC3-II reflects starvation-induced autophagic activity,

and detecting LC3 by immunoblotting or immunofluorescence has become a reliable method for

monitoring autophagy and autophagy-related processes, including autophagic cell death [76].

Figure 1.2 Primary mechanism of autophagy. Nucleation of the phagophore occurs following induction by the ULK1/2 complex. Elongation of the phagophore is aided by the ATG proteins. Eventually, the expanding membrane closes around its cargo to form an autophagosome and LC3-II is cleaved from the outer membrane of this structure. The outer membrane of the autophagosome will then fuse with the lysosomal membrane to form an autolysosome. The contents of the autolysosome are then degraded and exported back into the cytoplasm for reuse by the cell [161].

1.3.2. Functional forms of Autophagy

In response to stress induced by chemotherapy or radiation, four functional forms of autophagy have been identified: these are cytoprotective, cytotoxic, nonprotective, and cytostatic autophagy [77]. *Cytoprotective* autophagy, one of the best-known forms, is a pro-survival function that allows cells to endure conditions such as serum starvation or hypoxia [72]. Given that induction of cytoprotective autophagy decreases sensitivity to cancer drugs and treatment, pharmacological and genetic inhibition of autophagy increases sensitivity to the anticancer treatment that promotes the autophagy, which is a potential therapeutic strategy [78]. In response to chemotherapy and radiation, cells can also undergo a *cytotoxic* form of autophagy, resulting in reduced cell viability and clonogenic survival. Cytotoxic autophagy can kill tumor cells through both apoptosis-dependent and -independent mechanisms [79], [80]. In the case of *cytostatic* autophagy, therapy-induced growth inhibition and sensitivity is mediated through autophagy, rather than apoptosis; furthermore, autophagy interference restores cellular proliferation and ameliorates antitumor therapeutic effects and may also be associated with senescence [72], [81]. Finally, the less-known *nonprotective* form of autophagy is a form that may be induced by chemotherapeutic treatment, but autophagy inhibition does not alter tumor cell sensitivity to chemotherapy and radiation [82]–[84]. For example, studies demonstrated a low extent of apoptosis in response to radiotherapy in H460 NSCLC cells; however, the cells exhibited an increase in autophagy induction [84]. The precise significance of this form is yet to be determined since its advantage to the cell under stress conditions remains unclear [85].

1.4. Apoptosis

One of the main goals in treating castration-resistant prostate cancer and many other malignancies is to induce cell death. Apoptosis, the most renowned form of programmed cell death, operates as a key physiological mechanism that limits cell population expansion, either to maintain tissue homeostasis or to remove potentially harmful cells, such as those that have sustained DNA damage [86]. Apoptosis is fundamentally distinct from other types of cell death based on its incidence, morphology, and biochemistry. Morphological alterations of apoptotic cells include nuclear condensation and fragmentation, cell shrinkage, dynamic membrane blebbing, and loss of adhesion to extracellular matrices or to neighbors [87]. Biochemical alterations consist of chromosomal DNA cleavage into internucleosomal fragments, phosphatidylserine externalization, and activation of a family of proteases recognized as the caspases [88].

In mammals, there are two central apoptotic pathways: the extrinsic pathway (death receptor mediated pathway) and the intrinsic pathway (mitochondrial mediated pathway) [89]. Apoptotic signaling through the extrinsic pathway begins with the attachment of extracellular ligands, for example, tumor necrosis factor (TNF), Fas ligand (Fas-L), and TNF-related apoptosis-inducing ligand (TRAIL) to the extracellular domain of death receptors with the best-known receptors being the type 1 TNF receptor (TNFR1) and Fas (also called CD95/Apo-1) death receptors [90], [91]. Upon binding of ligand to receptor, the death receptors bind via their intracellular death domain with a corresponding protein motif in adapter proteins such as Fas-associated death domain (FADD) and TNF receptor-associated death domain (TRADD) [92]. Then, a death-inducing signaling complex (DISC) is developed, leading to auto-catalytic activation of procaspase-8 [93]. Active caspase-8 activates effector/executioner caspases, which cause cell death by damage or destruction of the nucleus and other intracellular structures [90].

In addition to external stimuli, apoptosis can also be regulated or activated by the mode of internal stimuli such as DNA damage and oxidative stress [94]. There are two main groups of the Bcl-2 proteins, namely the pro-apoptotic proteins (e.g. Bax, Bak, and Bad) and the anti-apoptotic proteins (e.g. Bcl-2, Bcl-xl, Bcl-w, and Mcl-1) present on the mitochondrial membrane, which are the key mediators for the intrinsic apoptotic pathway[95]. Pro-apoptotic protein activity leads to release of cyt. c (cytochrome c) in the cytoplasm after mitochondrial membrane perturbation. Released cyt. c in the cytoplasm forms a complexa called an apoptosome with apoptotic protease activating factor 1 (APAF1) and procaspase 9. This complex cleaves procaspase-9 to caspase 9, which then cleaves and activates the caspases of the executioner pathway such as caspase-3, -6, and -7 to induce cell death [96].
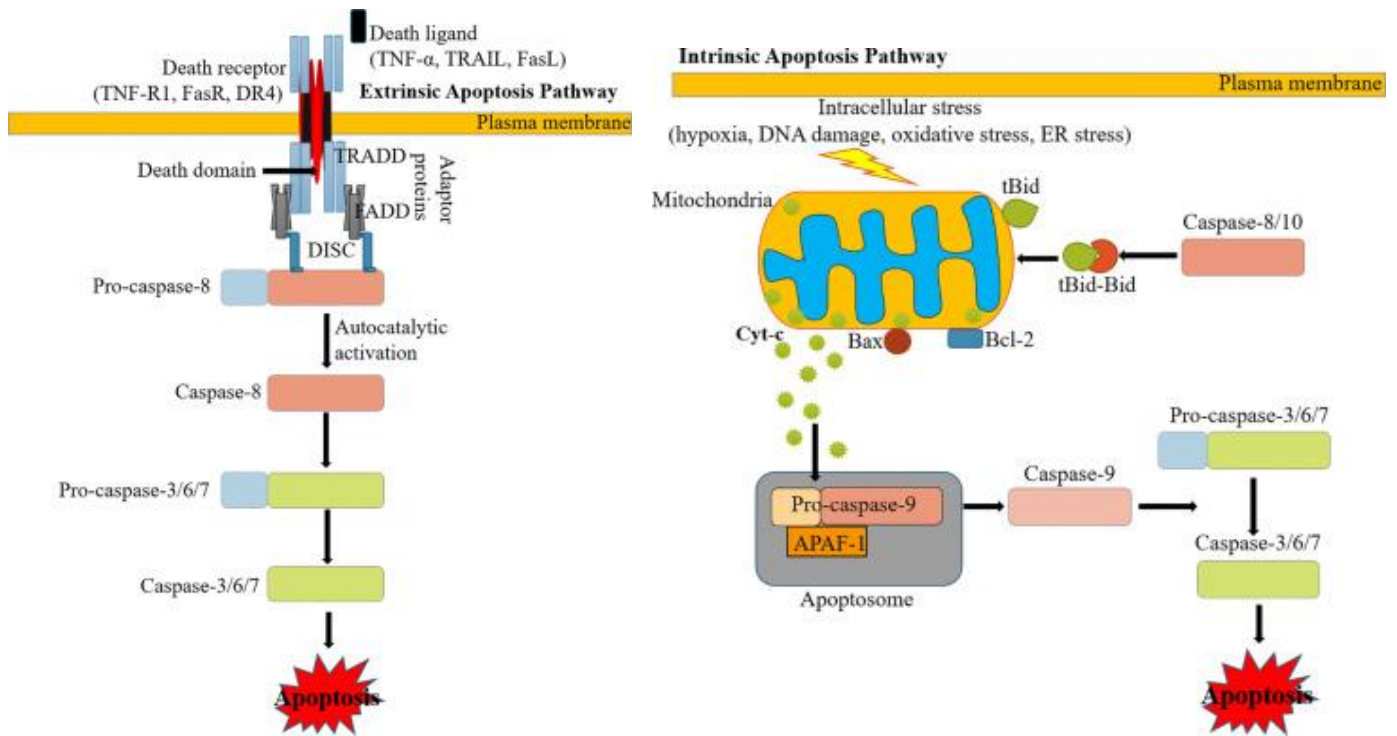
Figure 1.3 The Extrinsic and Intrinsic Apoptotic Pathways. In the extrinsic pathway, death ligands (TNF-α, TRAIL and FasL) recognize and bind to the death receptors (THN-R1, FasR, and DR4) causing the recruitment of adaptor proteins (FADD, TRADD) and form the DISC complex towards the cytoplasmic side. The formed DISC complex induces the autocatalysis of inactive pro-caspase-8 into active caspase-8. Subsequently, activated caspase-8 cleaves and activates caspase-3. Activated caspase-3 then induces apoptosis of target cell. In the intrinsic pathway, different cellular stress including hypoxia, DNA damage, and endoplasmic reticulum stress (ER) signal the pathway. Following the signal, the mitochondria releases Cyt. c into the cytoplasm which forms the apoptosome complex. The formed apoptosome further recruits and activates the executioner caspase-3 [162].

1.5. BET Protein Family

Bromodomain-containing protein 4 (BRD4), along with BRD2, BRD3, and testes/oocyte-specific BRDT, constitutes the bromodomain and extraterminal (BET) protein family in mammals [97], [98]. At the molecular level, these proteins act as epigenetic readers to specifically recognize acetylated lysine on histones, and biologically, the BET family is implicated in a broad spectrum of cellular processes such as cell proliferation, differentiation, metabolism, and DNA repair [99]–[101]. BRD4, the best-characterized member of the BET family, is described as a general regulator for RNA polymerase II (Pol II)–dependent transcription through interaction with positive transcription elongation factor (P-TEFb)[102]. Upon analyzing the genomic landscape, it has been observed that BRD4 is consistently linked to nearly all active promoters and a substantial portion of active enhancers across diverse normal and transformed cell types [103], [104].

In line with its overall function in regulating transcription, BRD4 has been implicated in various pathological conditions, notably inflammation, obesity, and tumorigenesis. This includes midline carcinoma, acute myeloid leukemia, gastric cancer, and breast cancer [101], [105]–[107]. The tumorigenic capabilities of BRD4 primarily stem from its ability to facilitate transcription elongation of crucial genes, such as *c-MYC* and *BCL-2*, which play vital roles in regulating the cell cycle and apoptosis [108], [109]. As such, BET proteins are being pursued as novel targets for cancer treatment. Potent BET inhibitors with promising antitumor efficacy in several preclinical cancer models have been developed in recent years such as JQ1, a small molecule that occupies the bromodomain pocket of BET proteins with a high affinity in a manner that is competitive with acetylated histones [98], [110].

Although previous observations have shown promising results of BET inhibitors in interfering with BRD4 function, the effect of BET inhibitors such as JQ1 and OTX015 are reversible which causes the re-accumulation of BRD4 protein and incomplete suppression of MYC [111]. This has inspired the generation of novel BRD4 targeting molecules using PROTAC technology [112]. Proteolysis-targeting chimeras (PROTACs) are hetero-bifunctional small molecules employing E3 ligase ligands, fused via a flexible chemical linker to a ligand that recognizes the target protein [113]. Such molecules can recruit the target protein to the E3 ligase, elicit ubiquitination of the target protein which leads to its degradation through the ubiquitin-proteasome system (UPS) [114]. ARV-825 is a newly developed inhibitor using PROTAC technology, which conjugates OTX015 with an E3 ligase cereblon (CRBN). Administration of ARV-825 renders recruitment of BRD4 to cereblon and results in a rapid, efficient, and prolonged BRD4 degradation [112].

Chapter 2: Materials and Methods

2.1. Antibodies and Reagents

The following primary antibodies were used: BRD4 (Cell Signaling Technology, 13440); c-Myc (Cell Signaling Technology, 5605); cleaved-PARP (Cell Signaling Technology, 9541); B-actin (Cell Signaling Technology, 4970); p62 (Cell Signaling Technology, 5114); LC3B (Cell Signaling Technology, 2775); and GAPDH (Cell Signaling Technology, 2118). Secondary antibodies: Horseradish peroxidase (HRP)-conjugated secondary antibodies (Cell Signaling, anti-mouse, 7076S; anti-rabbit, 7074S).

2.2. Cell Lines and Culture Conditions

LNCaP cells were purchased through ATCC, and PC3 and DU145 cells were graciously provided by Dr. Zheng Fu at Virginia Commonwealth University (Richmond, Virginia, USA). DU145 cells were grown in DMEM (Thermo Fisher, Waltham, MA, USA) with 10% (v/v) fetal bovine serum (FBS, Gemini Bio, West Sacramento, CA, USA) and 100 U/ml penicillin G sodium/100 μg/ml streptomycin sulfate (Thermo Fisher, Waltham, MA, USA). PC3 cells were grown in DMEM/F-12 (Thermo Fisher, Waltham, MA, USA) with 10% (v/v) fetal bovine serum (FBS, Gemini Bio, West Sacramento, CA, USA) and 100 U/ml penicillin G sodium/100 μg/ml streptomycin sulfate (Thermo Fisher, Waltham, MA, USA). LNCaP cells were grown in RPMI (Thermo Fisher, Waltham, MA, USA) with 10% (v/v) FBS, 1% non-essential amino acids (Thermo Fisher, Waltham, MA, USA), and 100 U/ml penicillin G sodium/100 μg/ml streptomycin sulfate (Thermo Fisher, Waltham, MA, USA).

For drug treatments, Palbocilib (LC Labratories, P-7788), Enzalutamide (Enza, APExBio, Houston TX, USA), ABT-263 (AbbVie, Chicago, IL, USA), ARV-825 (Med-chem express, HY-

16954), Abiraterone Acetate (Med-chem express, HY-75054), and 10058-F4 (Med-chem express, HY-12702) were dissolved in DMSO and administered in the dark at the appropriate concentrations and time. Docetaxel (Doc) was graciously provided by Dr. Zheng Fu and S63845 by Dr. Anthony Faber at Virginia Commonwealth University (Richmond, Virginia, USA). The concentrations of the drugs being utilized in this study have been selected based on the literature as well as screening studies performed in the Dr. Gewirtz laboratory. For charcoal-stripped conditions (CS-FBS, Thermo Fisher, Waltham, MA, USA), cells were maintained in normal medium with 10% charcoal-stripped serum as opposed to traditional FBS.

2.3. Cell Viability and MTS Assays

For viable cell counts and time course assays, cells were seeded at a known density $(2*10^4$ cells 6-well plate) and allowed to adhere overnight or for 48 hours. For all time courses, day 0 (D0) indicates the start of treatment. Viable cell counts were taken on a manual hemocytometer at the indicated times for each experiment.

For MTS assays, cells were plated in 96-well plates, in suitable concentrations, treated under the indicated conditions. The viability was assessed by UV spectrophotometer using MTS reagent (AB197010).

2.4. Promotion of Apoptosis

The extent of apoptotic cell death was measured using Annexin V-FITC/Propidium iodide staining. On the indicated day, cells were trypsinized, washed with 1X PBS and stained according to manufacturer protocol (Annexin V-FITC Apoptosis Detection Kit; BD Biosciences, 556547). All flow cytometry quantification was performed on the BD FACSCantoII cytometer, and at least 10,000 events were analyzed per sample. All experimental protocols were performed with cells protected from light.

2.5. SA-ß-gal staining

SA-β-Gal expression was assessed by X-Gal (Thermo Fisher, Waltham, MA, USA) histochemical staining and/or C12FDG (Thermo Fisher, Waltham, MA, USA) fluorolabeling and flow cytometry-based quantification. Both procedures were performed as previously described [115]. All images were taken using a 20X objective on an Olympus inverted 132 microscope IX70, with a Q-Color3TM Camera.

To quantify ß-gal positive senescent cells, after treatment, cells were treated with Bafilomycin A1 (100 nM) for 1 h to achieve lysosomal alkalinization, followed by staining with C12FDG (10 μM) for 1 h at 37 °C. All flow cytometry quantification was performed on the BD FACSCantoII cytometer, and at least 10,000 events were analyzed per sample.

2.6. Western Blotting

Protein was collected in CHAPS-lysis buffer containing protease and phosphatase inhibitors, and then quantified by the Bradford assay. Equal amounts of protein were prepared in SDS sample buffer, boiled, and then loaded into an SDS-polyacrylamide gel. Following electrophoresis, proteins were transferred in 10–20% methanol to a polyvinylidene difluoride membrane. Membranes were blocked in 5% bovine serum albumin (BSA) in PBS with 0.1% Tween-20, and then incubated overnight at 4°C with the indicated primary antibodies at a dilution of 1:1000 in 5% BSA. Membranes were washed, and then probed with secondary antibody at a dilution of 1:2000 in 5% BSA for 2h at room temperature. Protein was visualized with the Pierce ECL imaging kit (Thermo Fisher, Waltham, MA, USA) on BioRad ChemiDoc System.

2.7. Acridine Orange Staining

On the indicated days, cells were stained with 1 μg/ml acridine orange at 37°C for 20 min and then washed with 1X PBS. Cells were imaged using an inverted fluorescence microscope (Olympus, Tokyo, Japan) at 20X magnification.

2.8. High speed live cell interferometry (HSLCI)

HSLCI utilizes a custom inverted microscope setup with a wide field phase detection camera coupled to light emitting diode, as previously described [116], [117]. Motorized stages hold a standard glass bottom plate, while a piezo actuated autofocusing system maintains focus during scanning. The detected phase change in the light is then used to calculate the mass of single cells and cell clusters. Cells were plated at $0.5\text{-}1*10^4$ on a glass-bottomed six well plate (Cellvis, Mountain View, CA, USA) and treated with the respective conditions before monitoring for 12 hours. For measuring median growth, only cell clusters whose standard error in exponential or linear growth was less than 0.1% were included. Cell density was measured in the same cell clusters. After automated segmentation, the median biomass divided by the area (density) for the first ten loops (90 min of measurement) was taken to determine the density of each cluster at the beginning of the experiment.

2.9. Statistics

Unless otherwise indicated, all quantitative data is shown as mean ± SEM from at least three independent experiments, all of which were conducted in triplicates or duplicates. GraphPad Prism 9.0 software was used for statistical analysis. All data was analyzed using either one-way ANOVA with Tukey or Dunnet post hoc, or two-way ANOVA with Sidak or Dunnet post hoc, as appropriate. For all statistics, significance threshold was set at $p \leq 0.05$.

Chapter 3: The use of senolytics to increase the effectiveness of standard of care treatment for castration resistant prostate cancer

3.1. Introduction

Prostate cancer (PCa) is the most frequently diagnosed cancer in males and the second most common cause of cancer deaths with about 34,000 men dying each year in the U.S [1], [2]. The standard of care for advanced PCa is androgen deprivation therapy (ADT); however, an initial response followed by a progressive rise in PSA gives rise to castration-resistant prostate cancer (CRPC). It is important to note, especially for this research, that the term "castration resistant" is preferred over the previously used designations of "androgen independent" and "hormone refractory" disease because, despite absence of circulating testosterone, the tumor remains functionally dependent on androgens and on the androgen receptor, though the disease can eventually progress to being "androgen independent" [6]. This is relevant to the standard of care therapy currently utilized in the clinic, which includes anti-androgens enzalutamide and abiraterone alongside docetaxel and ADT. In theory, the antiandrogens should not be effective in cells that lack androgen receptors due to the antagonist actions of these drugs at these receptors; however, given the clinical utilization of these agents in castration resistant prostate cancer, it is clear that some androgen-associated signaling pathways remain functional. Unfortunately, there are currently no appropriate cell lines available that are both castration resistant and that express the AR, even though androgen deprivation is effective, at least temporarily, in the treatment of the castration resistant disease [118]. The primary CRPC cell lines used in this research and in the scientific literature relating to "castration-resistant" prostate cancer are DU145 and PC3 cells; both cell lines lack androgen receptors and are p53 deficient while DU145 cells are also Rb

deficient. PC3 is a cell line from grade IV adenocarcinoma with high metastatic potential while DU145 is a cell line from prostate carcinoma, with moderated metastatic potential [119].

3.1.1. Senescence in response to enzalutamide in CRPC

The role of therapy-induced senescence using enzalutamide in androgen-independent cell lines is not well documented. Malaquin et al. did generate extensive data in the androgen-dependent LNCaP cells using DNA-damaging agents as well as enzalutamide in combination with senolytics [120]. The DNA damage inducers, irradiation and Olaparib, which is a PARP inhibitor inhibiting poly ADP ribose polymerase, an enzyme involved in DNA repair, triggered classical therapy-induced senescence (TIS) in PCa cells in addition to the mitotic catastrophe and cell death observed in PC3 cells. Mitotic catastrophe is a mode of cell death that results from premature or inappropriate entry of cells into mitosis and can be caused by chemical or physical stresses [121]. Enza also induced TIS in LNCaP cells in the absence of direct DNA damage. In addition to the absence of DNA damage, these investigators showed that Enza-TIS cells did not share other senescence-associated (SA) markers observed in XRA- or Olap-senescent cells; specifically, the LNCaP cells displayed: a more gradual loss of DNA synthesis with an accumulation of cells in G1 phase; no more than 30% SA-β-gal positive cells; a complete absence of additional DNA damage foci or genomic instability; increased p16 but not p21 expression, and a reversible proliferation arrest. Although p16 expression is often associated with an irreversible state of senescence [122], [123], Enza treatment for more than 30 days sustained a senescence that was rapidly reversible upon drug removal, suggesting that Enza-TIS depends on different underlying molecular mechanisms for both induction and maintenance when compared to DNA damage-TIS [120].

Furthermore, while senolytics in the Bcl-2 family of anti-apoptotic inhibitors such as ABT-263 were lethal for PCa-TIS cells with evidence of DNA damage, they were ineffective against enzalutamide-TIS cells. This study laid the groundwork for a deeper investigation into enzalutamide in androgen independent cell lines as well as the effectiveness of other types of potential senolytics.

3.1.2. BET inhibition and its potential for senolytic use

There have been recent studies looking at the potential for use of epigenetic regulators in cancer research [124]. Epigenetic regulators change the expression of genes rather than the code itself [125]. In cancer, many of these proteins involved in regulation of transcription are elevated [126]. These include the bromodomain and extra terminal (BET) protein family, which includes BRD2, BRD3, and BRD4 among others. BET proteins function by binding to acetylated lysine residues on histone proteins important for regulating transcription [127]. BET inhibition has demonstrated efficacy in pre-clinical studies and is being evaluated in various clinical trials for both hematological malignancies and solid tumors [128]; these include the inhibitors JQ1 [129], OTX015 [130], ABBV-075 [131], and ARV-825 [132] among many others. Further studies have shown that BET inhibitors such as JQ1 and ARV-825 have possible senolytic activity using different experimental cancer models [133].

3.1.3. Overarching Hypotheses

Different treatment modalities including antiandrogens and chemotherapy have been shown to induce a transient remission for those with CRPC; however, eventually, there is a recurrence of the disease in most patients. In other experimental models, the use of senolytics to

improve the response to cancer therapy has been successful [54], [134], [135]. Consequently, we hypothesized that the use of these senolytics could be possible strategies to increase the effectiveness of some of the current standards of care therapy for castration-resistant prostate cancer, especially enzalutamide.

3.2. Results

3.2.1. Screening for concentrations from dose-response curves of anti-androgen and senolytic drugs on DU145 and PC3 cell lines

Initially, dose-response studies were performed using an MTS assay for both DU145 and PC3 cell lines to determine the concentrations of anti-androgens and senolytics agents to utilize in the subsequent work. Figures 1A through 1D show the effect of anti-androgens, enzalutamide and abiraterone acetate, as well as the putative senolytics, ARV-825 and ABT-263, respectively, for the DU145 cell line. In Figures 1A and B, DU145 cells were plated at a 4000 cell per well density based on previous dilutions and each drug was screened for 72 hours in a dose range of 0 to 100 μM. In Figure 1C, DU145 cells were plated at a 2000 cell per well density and screened for 96 hours in a dose range of 0 to 500 nM for ARV-825. Figure 1D demonstrates the effects of the senolytic, ABT-263; DU145 cells were plated at a 5000 cells per well density and screened for 48 hours in a dose range of 0 to 10 μM. Treatment durations and ranges were decided based on previous work in this laboratory and others [56], [120], [135]–[137].

Figures 2A-D show the same dose-response screens for the PC3 cell line as for the DU145 cells. The IC-50 values for enzalutamide were determined to be 58.5 μM and 37.09 μM for the PC3 and DU145 cells, respectively; for comparison, the IC-50 value for enzalutamide in LNCaP cells is 5.6 μM [138].

After examining the dose response curves for the anti-androgen drugs, concentrations of 50 and 100 μM were initially chosen to be utilized in further experiments for both enzalutamide and abiraterone acetate as they had the most relevant effects based on the curves; however, this was modified in subsequent studies, as indicated below. While ABT-263 is heavily used in our lab even at concentrations that don't have antiproliferative effects alone, it was not logical to continue its use in combination with Enza treated cells in this case. As explained from Malaquin et al., they found that inhibitors of the Bcl-2 antiapoptotic family, ABT-263 and A-115, which targets selectively Bcl-xL, were strongly efficient to kill XRA- and Olap-TIS cells but not Enza-TIS cells [120]. The mechanism underlying this latter phenomenon remains unclear but the authors suggested that DNA damage is key for sensitization to Bcl-2 family senolytics [120].
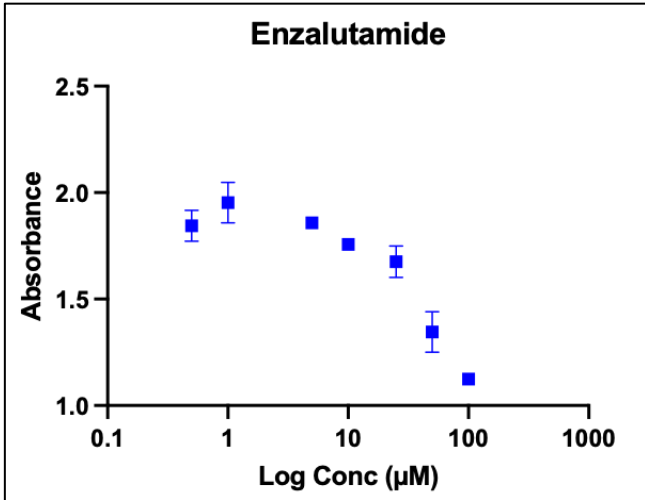
Figure 1A

DU145 cells were plated at a 4x10^3 concentration in 96 well plates and treated with enzalutamide for 72 hours after being left overnight to adhere. The MTS assay was observed in a dose range of 0 to 100 μM and absorbances were determined using a UV plate reader. Data represent means ± standard errors for three experiments.
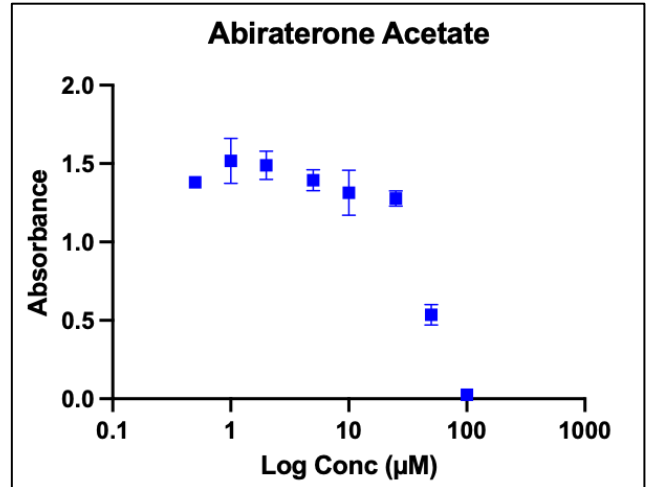

Figure 1B

DU145 cells were plated at a 4x10^3 concentration in 96 well plates and treated with abiraterone acetate for 72 hours after being left overnight to adhere. The MTS assay was observed in a dose range of 0 to 100 μM and absorbances were determined using a UV plate reader. Data represent means ± standard errors for three experiments.
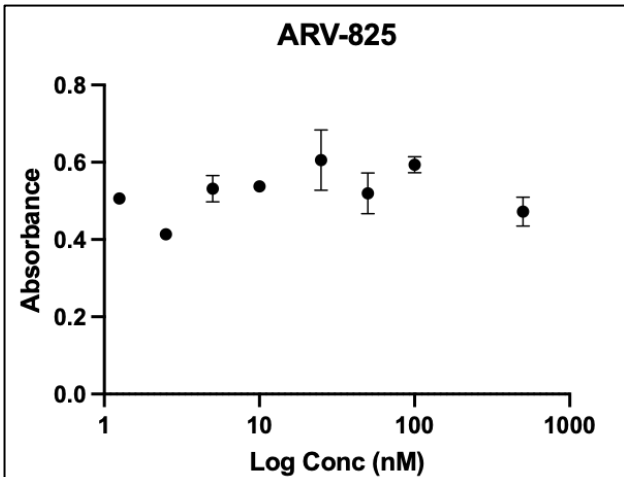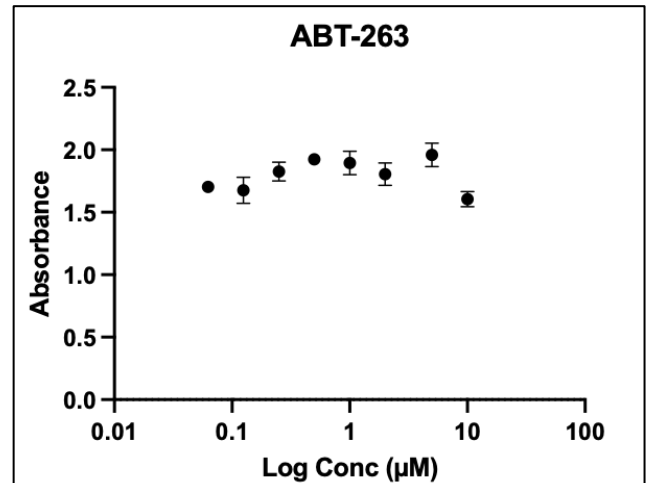

Figure 1C

DU145 cells were plated at a 2x10^3 concentration in 96 well plates and treated with ARV-825 for 96 hours after being left overnight to adhere. The MTS assay was observed in a dose range of 0 to 500 nM and absorbances were determined using a UV plate reader. Data represent means ± standard errors for three experiments.

Figure 1D

DU145 cells were plated at a 5x10^3 concentration in 96 well plates and treated with ABT-263 for 48 hours after being left overnight to adhere. The MTS assay was observed in a dose range of 0 to 10 μM and absorbances were determined using a UV plate reader. Data represent means ± standard errors for three experiments.

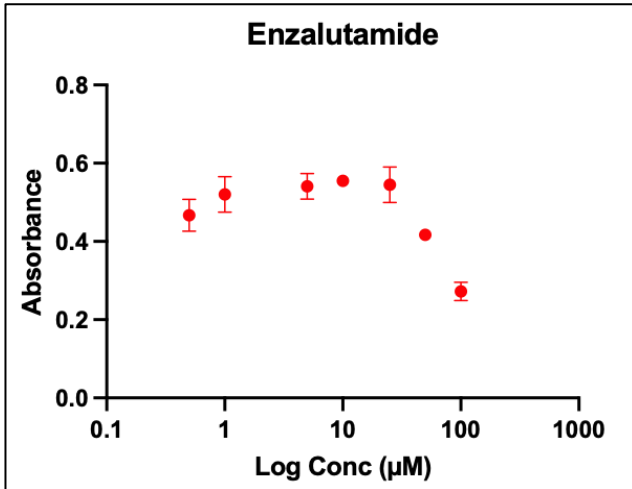**Figure 2A**

PC3 cells were plated at a 4x10^3 concentration in 96 well plates and treated with enzalutamide for 72 hours after being left overnight to adhere. The MTS assay was observed in a dose range of 0 to 100 μM and absorbances were determined using a UV plate reader. Data represent means ± standard errors for three experiments.
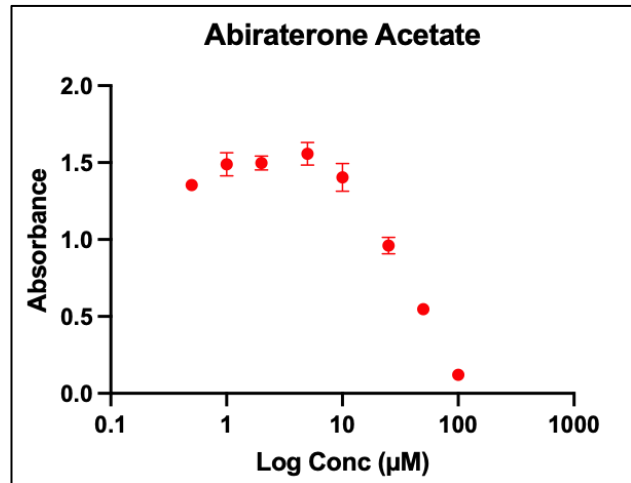

Figure 2B

PC3 cells were plated at a 4x10^3 concentration in 96 well plates and treated with abiraterone acetate for 72 hours after being left overnight to adhere. The MTS assay was observed in a dose range of 0 to 100 μM and absorbances were determined using a UV plate reader. Data represent means ± standard errors for three experiments.
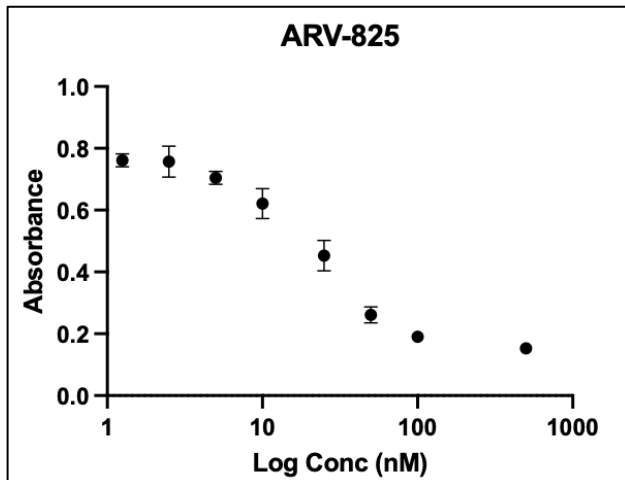

Figure 2C

PC3 cells were plated at a 2x10^3 concentration in 96 well plates and treated with ARV-825 for 96 hours after being left overnight to adhere. The MTS assay was observed in a dose range of 0 to 500 nM and absorbances were determined using a UV plate reader. Data represent means ± standard errors for three experiments.

Figure 2D

PC3 cells were plated at a 5x10^3 concentration in 96 well plates and treated with ABT-263 for 48 hours after being left overnight to adhere. The MTS assay was observed in a dose range of 0 to 10 μM and absorbances were determined using a UV plate reader. Data represent means ± standard errors for three experiments.
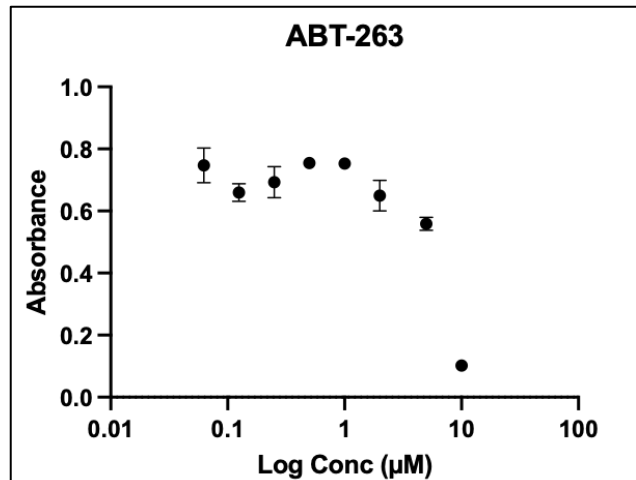
3.2.2. Enzalutamide and abiraterone acetate produce a growth arrest response at high, but not clinically relevant concentrations in DU145 and PC3 cells

Studying these drugs further was considered to be a useful preclinical strategy given the extensive clinical usage of enzalutamide and abiraterone acetate for CRPC in addition to the lack of robust data with these drugs in androgen independent cells. The present studies were performed to determine the influence of enzalutamide and abiraterone acetate on growth and viability in prostate tumor androgen independent cell lines, PC3 and DU145. Although 50 and 100 μM were higher than the clinically relevant dosages for both drugs, studies in LNCaP95 enzalutamide-resistant cells using 50 μM of enzalutamide provided justification for continuing the use of these higher concentrations in cells that would likely be resistant to enzalutamide at lower dosages [139].

Figures 3A and 3B present a determination of viable cell number using a time course assay in DU145 cells on the indicated days after exposure to 50 and 100 μM enzalutamide and abiraterone acetate, respectively, for 72 hours and fresh media was replenished after drug removal on day 3.

Figures 4A and 4B present a determination of viable cell number using a time course assay in PC3 cells on the indicated days after exposure to 50 and 100 μM enzalutamide and abiraterone acetate, respectively, for 72 hours, where fresh media was replenished after drug removal on day 3.

Given that enzalutamide acts an antagonist for the androgen receptor (AR), the results were expected to be negative since both PC3 and DU145 cell lines are AR independent [140]. Interestingly, for both cell lines with enzalutamide, there appeared to be a significant growth delay effect from the 100 μM concentration and a less significant effect from the 50 μM

concentration with DU145 cells appearing to have less viability compared to the PC3 cells at this dosage. Having said that, 100 μM is not a clinically relevant dosage for enzalutamide as it is much higher than the circulating blood concentration in humans and may be showing off target, toxic effects to the cells [141].

Similarly for abiraterone, the active metabolite of abiraterone acetate, it is a partial antagonist for AR in addition to being an inhibitor for CYP17A1, which wouldn't be expected to factor into *in vitro* studies in these cell lines as CYP17A1 is found in prostatic tumor tissues *in vivo* [142]. Nevertheless, the abiraterone acetate had significant growth delay effects to the point that almost all the cells were decimated and did not recover at each of the concentrations for each cell line. This is highly likely due to off target effects and toxicity and the concentration of abiraterone acetate would need to be significantly lowered in future studies.

After examining this time course data in addition to previous data, it was determined that the cells should be grown for 48 hours prior to treatment with any of the drugs since normally, in the clinic, tumors are growing when treated. Furthermore, given the blood circulating concentration of enzalutamide being in the range of 1- 35 μM, it was evident that a lower concentration would be more clinically relevant [141]. Figure 4C shows PC3 cells being treated with enzalutamide for 72 hours at 25 and 50 μM after having grown for 48 hours prior to treatment using a time course assay for cell viability. Both the 25 and 50 μM concentrations had limited effects on the growth of the cells and any growth delay was minimal in the PC3 cells with the 50 μM dosage having a slightly greater dose dependent effect. DU145 data with the lower concentrations of enzalutamide is not shown as PC3 cells were chosen as the main cell line of focus for the research at this point. We had decided that emphasizing studies in the PC3 cells, which seemed to have a slightly greater response to enzalutamide, would allow us to focus and

sharpen the hypothesis; however, we did come back to the DU145 cells later in the ARV-825 alone studies as a comparative cell line.

The time courses with the anti-androgens in Figures 3 and 4 showed clear evidence for growth arrest and therefore, the next logical step was determining whether this was due to senescence, which would allow these cells to be targeted by senolytics. One of the hallmarks of senescence is upregulation of beta-galactosidase, which can be visualized with an Xgal staining assay under a microscope. Figures 5A and 5B demonstrate the lack of senescence by β-gal staining with a 72 hour treatment of 50 and 100 μM enzalutamide and abiraterone acetate, respectively, on the indicated days as well as lack of morphological changes associated with senescence in DU145 cells. The DU145 cells showed no evidence of the blue-green stain that indicates upregulation of beta-galactosidase for either of the concentrations for either Enza or AA. Flow cytometry data to quantify senescence in this cell line was inconclusive and not included due to potential growth issues with the cell line at that time.

Like Figure 5, Figures 6A and 6B were stained after being treated for 72 hours with 50 and 100 μM enzalutamide and abiraterone acetate, respectively, on the indicated days for PC3 cells. Furthermore, the CDK4/6 inhibitor, Palbociclib was used as a positive control in these cells as shown in Figure 6C; PC3 cells were treated with 1 μM Palbociclib for 6 days alongside cells treated with 50 μM enzalutamide for 6 days and an untreated control. The cells in Figures 6A and 6B showed minimal blue-green staining and upregulation of beta-galactosidase in PC3 cells for both Enza and AA though there were some flattened and enlarged morphological changes in the cells that were stained.

To quantify the level of senescence, C12FDG flow cytometry was used to sort the senescent cells based on fluorescence signal after staining. Figure 6D shows the percentage of

senescent cells in PC3 cells treated for 72 hours with enzalutamide at 25 and 50 µM as compared to untreated controls following the time course data from Figure 4C. We decided to try 25 µM and 50 µM instead of 50 and 100 µM at this point since the 100 µM dose was too high and cytotoxic; 25 µM was within the blood circulating concentration of enzalutamide in humans while 50 µM was around the IC50 of enzalutamide in PC3 cells. The flow data demonstrated a minimal induction of senescence following enzalutamide treatment in PC3 cells with a range of 7% to 13% senescent cells in the population compared to about 5% senescence in the controls, which is normal to see in cells [56], [120].

Taken together, these senescence data suggest that senolytics would likely have only a minimal effect on the cells treated with enzalutamide or abiraterone; however, given the mechanism of action of ARV-825, its effects may not be limited to cells that are in senescence as will be seen in the next section. ABT-263 only works in cells that are first induced into senescence so there wouldn't be any purpose in further pursuing it in combination with enzalutamide in PC3 cells [49], [56].
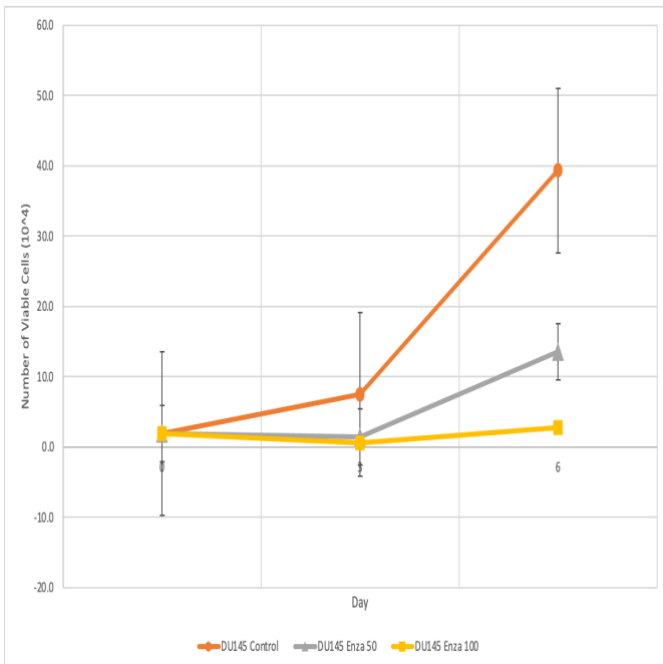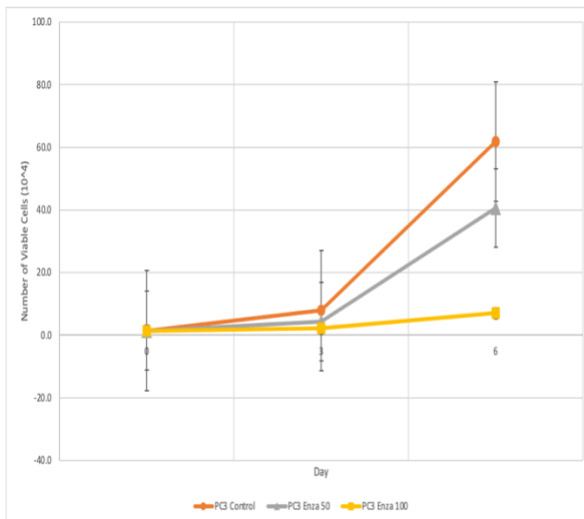

Figure 3A

DU145 cells were plated at a 2x10^4 concentration and left to adhere overnight before adding enzalutamide at 50 and 100 µM concentration to each well on day 0 and the drug was removed on day 3. The cells were counted for each condition at days 0, 3 and 6. Data represent means ± standard errors for three experiments.
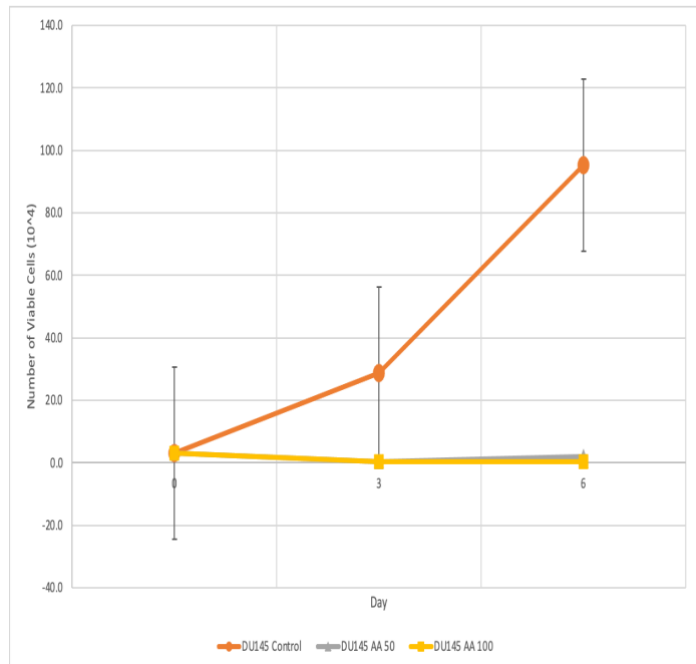
Figure 3B

DU145 cells were plated at a 2x10^4 concentration and left to adhere overnight before adding abiraterone acetate at 50 and 100 µM concentration to each well on day 0 and the drug was removed on day 3. The cells were counted for each condition at days 0, 3 and 6. Data represent means ± standard errors for three experiments.

Figure 4A

PC3 cells were plated at a 2x10^4 concentration and left to adhere overnight before adding enzalutamide at 50 and 100 µM concentration to each well on day 0 and the drug was removed on day 3. The cells were counted for each condition at days 0, 3 and 6. Data represent means ± standard errors for three experiments.
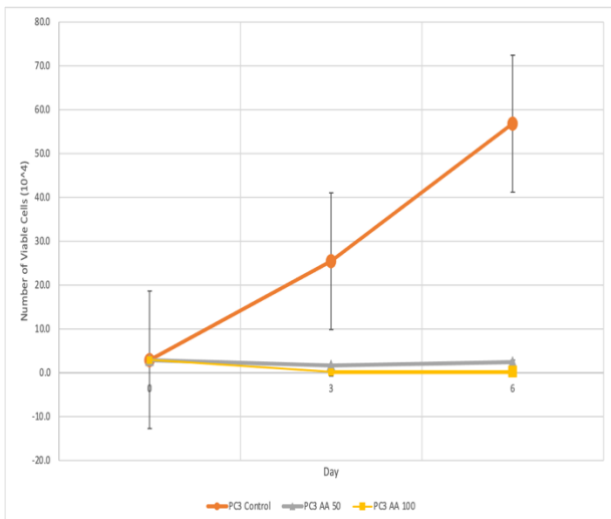

Figure 4B

PC3 cells were plated at a 2x10^4 concentration and left to adhere overnight before adding abiraterone acetate at 50 and 100 µM concentration to each well on day 0 and the drug was removed on day 3. The cells were counted for each condition at days 0, 3 and 6. Data represent means ± standard errors for three experiments.
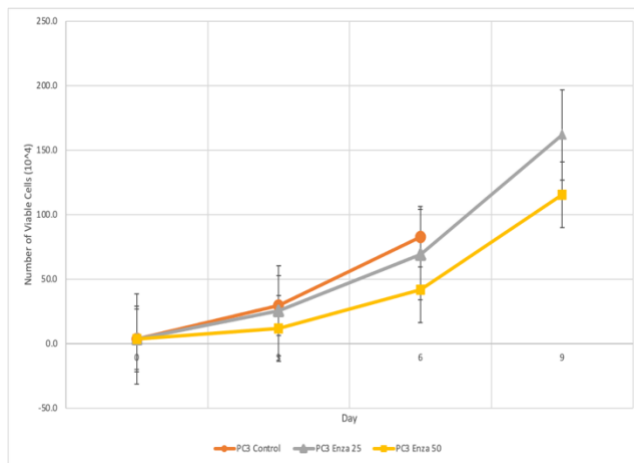

Figure 4C

PC3 cells were plated at a 2x10^4 concentration and left to grow for 48 hours before adding enzalutamide at 25 and 50 µM concentration to each well on day 0 and the drug was removed on day 3. The cells were counted for each condition at days 0, 3, 6 and 9. Data represent means ± standard errors for three experiments.
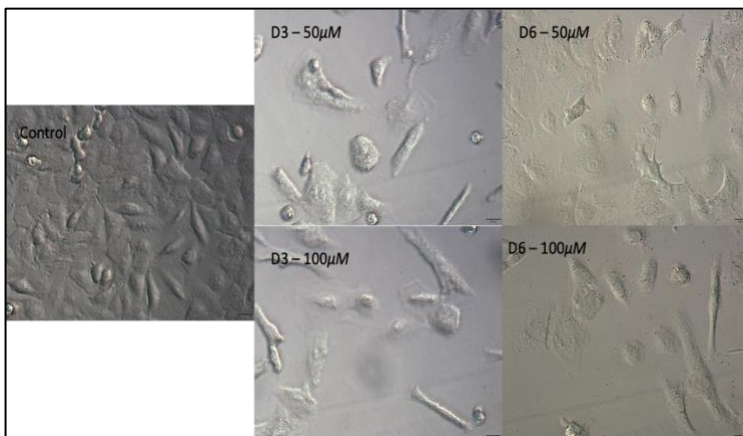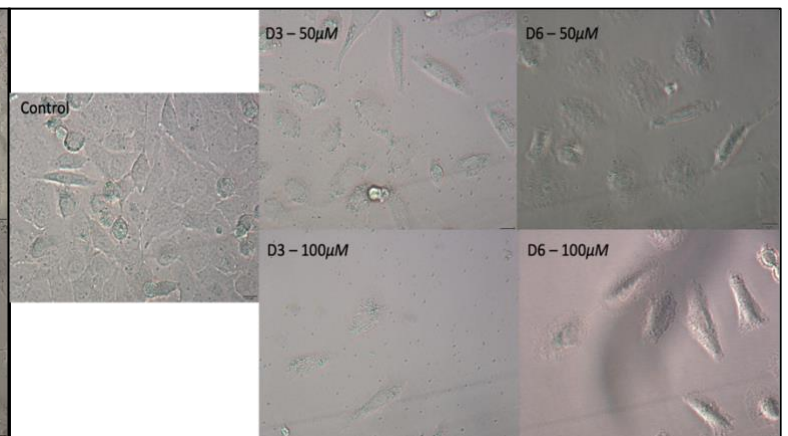

Figure 5A

DU145 cells were plated at a 2x10^4 concentration and left to adhere overnight before adding enzalutamide for 72 hours at 50 and 100 µM concentration to each plate on day 0. Cells were fixed on each of the indicated days, stained with x-gal staining solution and imaged using brightfield microscope. All images were taken at the same magnification.

Figure 5B

DU145 cells were plated at a 2x10^4 concentration and left to adhere overnight before adding abiraterone acetate for 72 hours at 50 and 100 µM concentration to each plate on day 0. Cells were fixed on each of the indicated days, stained with x-gal staining solution and imaged using brightfield microscope. All images were taken at the same magnification.
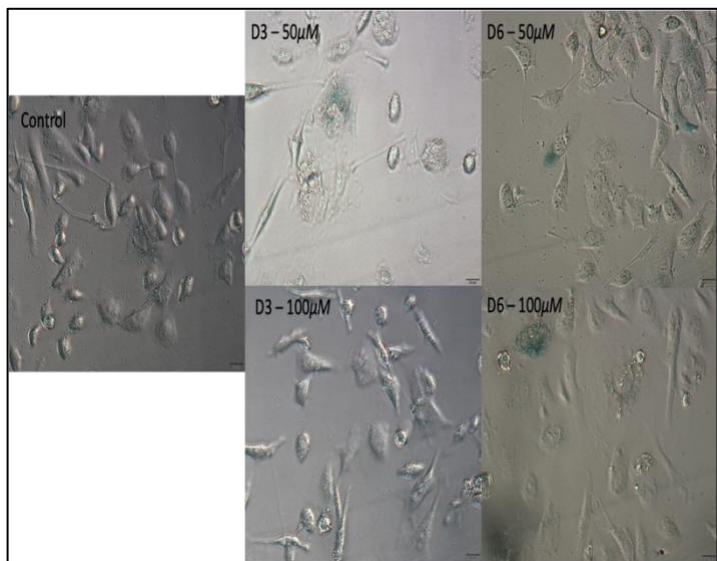
Figure 6A

PC3 cells were plated at a 2x10^4 concentration and left to adhere overnight before adding enzalutamide for 72 hours at 50 and 100 µM concentration to each plate on day 0. Cells were fixed on each of the indicated days, stained with x-gal staining solution and imaged using brightfield microscope. All images were taken at the same magnification.

Figure 6B

PC3 cells were plated at a 2x10^4 concentration and left to adhere overnight before adding abiraterone acetate for 72 hours at 50 and 100 µM concentration to each plate on day 0. Cells were fixed on each of the indicated days, stained with x-gal staining solution and imaged using brightfield microscope. All images were taken at the same magnification.
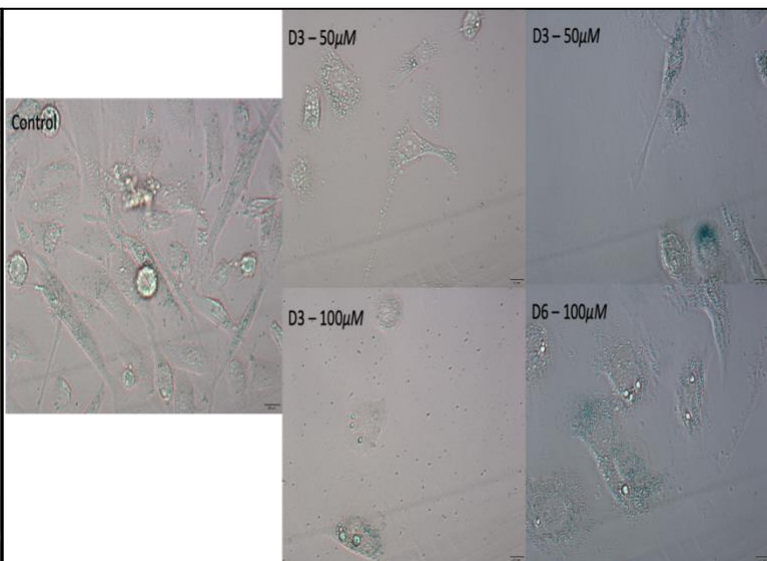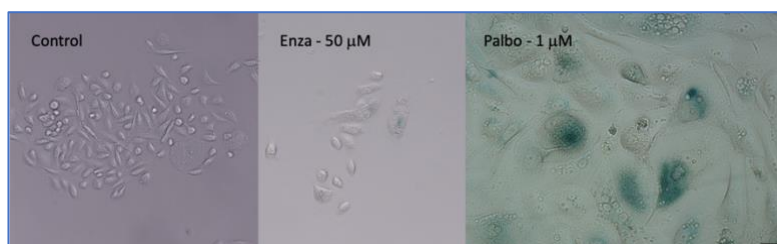

Figure 6C

PC3 cells were plated at a 2x10^4 concentration and left to adhere overnight before adding either 50 µM enzalutamide for 6 days or 1 µM Palbociclib for 6 days to the appropriate well on day 0. Each drug was replenished after 3 days. Cells were fixed on day 6, stained with x-gal staining solution and imaged using brightfield microscope. All images were taken at the same magnification.
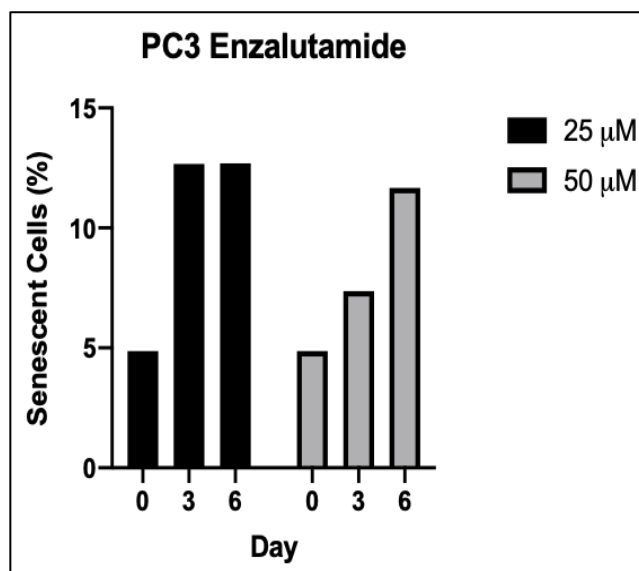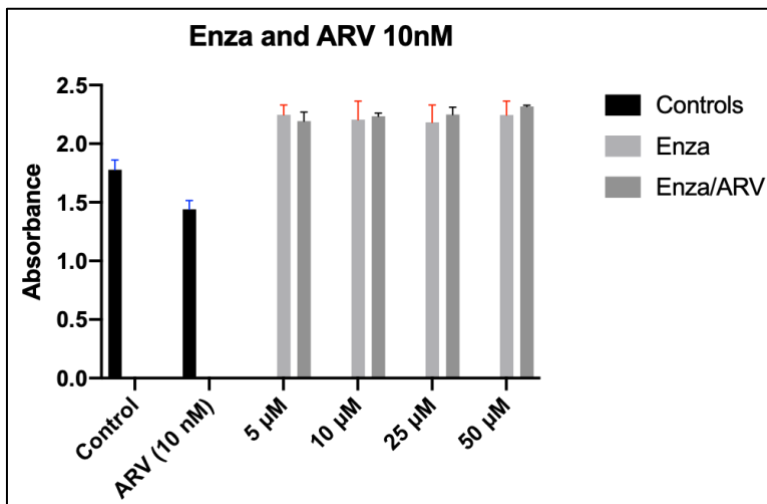

Figure 6D

PC3 cells were plated at a 2x10^4 concentration and left to grow for 48 hours before adding enzalutamide for 72 hours at 25 and 50 µM concentration to each plate on day 0. Cells were stained with C12FDG and then sorted into senescent and non-senescent populations using flow cytometry based on fluorescence signal.

3.2.3. ARV-825 fails to enhance the response to enzalutamide in PC3 cells but has a significant effect as a monotherapy

This laboratory has shown success in various models where cells induced into senescence can be targeted by senolytics and killed [49], [56], [135], [136]. Given that the PC3 cells had a dramatic response to ARV-825 as seen in Figure 4C, it was logical to explore this potential in combination with an anti-androgen such as enzalutamide. In an MTS assay in Figures 7A-C, PC3 cells were treated with enzalutamide for 72 hours in a dose range from 5 to 50 μM; ARV-825 was added to half these wells in combination after enzalutamide was removed as well as in several wells that weren't initially treated with enzalutamide. Each of the three plates was treated with a different concentration of ARV-825 (either 10, 25 or 50 nM).

From the data in Figures 7A-C, there are several significant observations that can be made. The most obvious observation is that in each of the Figures, the enzalutamide doesn't have a significant effect on its own nor does the combination with ARV-825 have any noticeable effect. While there was an effect of enzalutamide alone in the time course studies in the previous section as well as in the initial dose response curves at higher doses, these plates were run after 7 days to accommodate the treatment duration of ARV-825, which would likely allow the enzalutamide alone treated cells to recover from their arrest. In contrast, ARV-825 has a significant growth inhibitory or cytotoxic effect as a monotherapy despite not having any effect in the combination; this growth suppressive and/or cytotoxic effect also appears to increase in a dose dependent manner as the concentration of ARV-825 increases. The finding that enzalutamide may be affecting the (antitumor) mechanism of ARV-825 in these cells to the point where it is ineffective is significant and warrants further investigation in future studies. However, given the significance of ARV-825's dose-dependent effect alone, it was decided that this direction would be further pursued at this point.

Figure 7A

PC3 cells were plated in 96 well plates and grown for 48 hours before enzalutamide was added to select wells for 72 hours at day 0. Enzalutamide was removed on day 3 followed by addition of 10 nM ARV-825 to select wells for 96 hours. The doses for enzalutamide were 5, 10, 25, and 50 µM. The MTS assay absorbances were determined using a UV plate reader. Data represent means ± standard errors for three experiments.
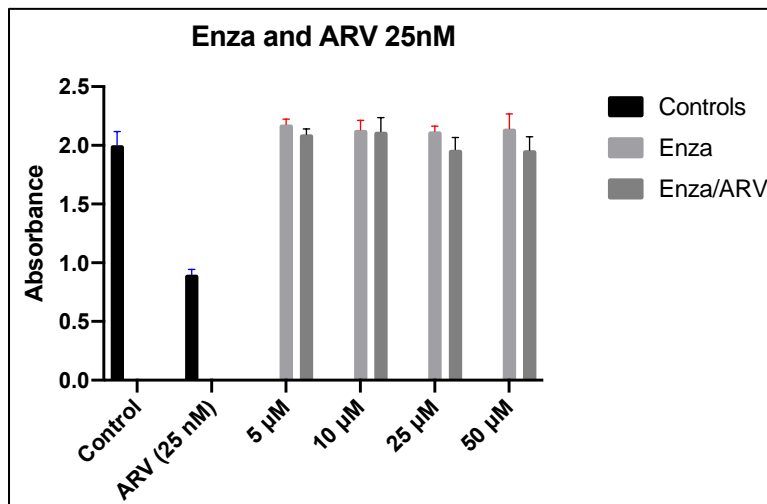
Figure 7B

PC3 cells were plated in 96 well plates and grown for 48 hours before enzalutamide was added to select wells for 72 hours at day 0. Enzalutamide was removed on day 3 followed by addition of 25 nM ARV-825 to select wells for 96 hours. The doses for enzalutamide were 5, 10, 25, and 50 µM. The MTS assay absorbances were determined using a UV plate reader. Data represent means ± standard errors for three experiments.

Figure 7C

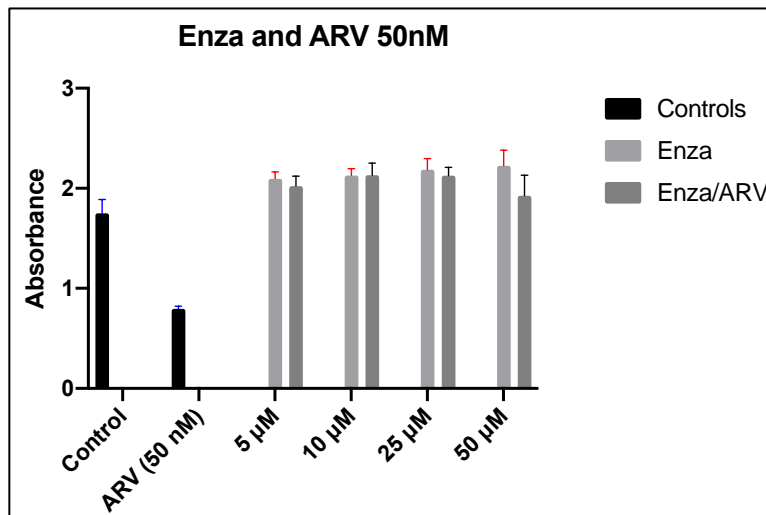PC3 cells were plated in 96 well plates and grown for 48 hours before enzalutamide was added to select wells for 72 hours at day 0. Enzalutamide was removed on day 3 followed by addition of 50 nM ARV-825 to select wells for 96 hours. The doses for enzalutamide were 5, 10, 25, and 50 µM. The MTS assay absorbances were determined using a UV plate reader. Data represent means ± standard errors for three experiments.

3.2.4. ARV-825 fails to enhance the response to enzalutamide in AR-dependent LNCaP cells

PC3 cells are known to be AR independent; given that enzalutamide acts on androgen receptors, there wasn't expected to be much of a response to enzalutamide alone [143]. Therefore, it seemed reasonable that this experiment should be repeated in an AR dependent cell line, in this case the p53 wild type LNCaP cell line. LNCaP is a cell line from prostate carcinoma with low metastatic potential [119]. The MTS experiment in Figures 7A-C was repeated with the exact same parameters except with the LNCaP cell line instead of the PC3 cells, with results shown in Figures 8A-C.

The data in the LNCaP cells yielded somewhat more predictable results. Like the PC3 cells, the ARV-825 had a significant and seemingly dose dependent effect as a monotherapy. However, as expected for an AR dependent cell line, the LNCaP cells exhibited a fairly dose dependent response to the enzalutamide alone and an even greater response in the combination of enzalutamide with ARV-825; however, the response in combination was not significantly greater than the response to ARV-825 alone, hence indicating that ARV-825 failed to enhance the response to enzalutamide. This observation is contradictory to data with ARV-825 in breast cancer models from our lab; the ARV-825 was able to sensitize the cells in these experiments [136]. It's likely that these androgen dependent cells weren't sensitized because of the transient form of senescence induced by enzalutamide; studies by Malaquin et al. in LNCaP cells showed that the senescence induced by enzalutamide was different than that of a DNA damaging agent and that this fact is key for sensitization to Bcl-2 family senolytics [120]. Taken together with Figure 7, when comparing the PC3 and LNCaP cells, there appeared to be evidence that some significant alteration regarding the mechanism of ARV-825 was occurring when enzalutamide

was added first in the AR independent cell line and perhaps even in the LNCaP cell line that would be able to explain why ARV-825 is not sensitizing these cells either.

One potential explanation for enzalutamide interfering with the effect of ARV-825 is that the enzalutamide is inducing the cells into a state of cytoprotective autophagy, making the ARV-825 ineffective and the cells able to survive [144]. To evaluate whether the PC3 cells are induced into a state of autophagy as a result of enzalutamide and/or ARV-825 treatment, acridine orange staining was utilized. The acridine orange emission color changes from yellow, to orange, to red in acidic environments, such as the lysosomes [145]. In this study, PC3 cells were treated with either 25 µM enzalutamide; 10, 25, or 50 nM ARV-825; or the combination of 25 µM enzalutamide with each of the ARV-825 concentrations. After each treatment ended, the cells were stained with acridine orange and visualized using a fluorescent microscope as seen in Figures 8D-J. From the images, it is apparent that there was in increase in autophagy for each condition including ARV-825 alone as compared to the control as well as significantly fewer cells; however, the combination appears to have the highest level of autophagy as seen from the high expression of red and morphological changes such as vacuolization and formation of the autophagosomes. Having said that, this would need to be quantified via flow cytometry to establish clear evidence that there was in increase in autophagy. These images serve as support that the enzalutamide and perhaps also the ARV-825 is inducing autophagy in the PC3 cells, especially in the combination.

Two proteins that can be examined to assess autophagy are p62 and LC3B [146]. In this study shown in Figure 8K, three different concentrations of enzalutamide (10, 25 and 50 µM), 50 nM of ARV-825 and the combination of ARV-825 with each of the enzalutamide concentrations were used in a western blot analysis assessing levels of p62 and LC3B. There appears to be some

p62 degradation in the combinations as well as enzalutamide alone at 50 μM, especially compared to the control and ARV-825 alone.

Endogenous LC3 is detected as two bands LC3-I, which is cytosolic, and the other LC3-II, which is conjugated with phosphatidylethanolamine (PE) and is present on isolation membranes and autophagosomes, and much less on autolysosomes [147], [148]. From the LC3 bands in Figure 8D, LC3-II accumulated for enzalutamide alone and even more in the combination. This indicates that the treatment causes either upregulation of autophagosome formation or blockage of autophagic degradation [149]. These two possibilities cannot be distinguished from the results shown in this part of the panel. The increase in LC3-II simply indicates the accumulation of autophagosomes but does not guarantee autophagic degradation. If, however, the amount of LC3-II further accumulates in the presence of lysosomal protease inhibitors, this would indicate enhancement of the autophagic flux (A1) [149]. However, if the LC3-II level were to remain unchanged, it is likely that autophagosome accumulation occurred due to inhibition of autophagic degradation; for example, blockage of autophagosome-lysosome fusion. Overall, this western blot analysis is inconclusive on its own and future experiments in the presence of lysosomal protease inhibitors may be useful to determine the extent of autophagy induced by enzalutamide and/or ARV-825. Taken together with the acridine orange staining data, there is evidence in support of autophagy induction; however, more studies would need to be conducted to confirm whether enzalutamide or ARV-825 is responsible for autophagy and what functional form of autophagy is present such as cytoprotective autophagy.
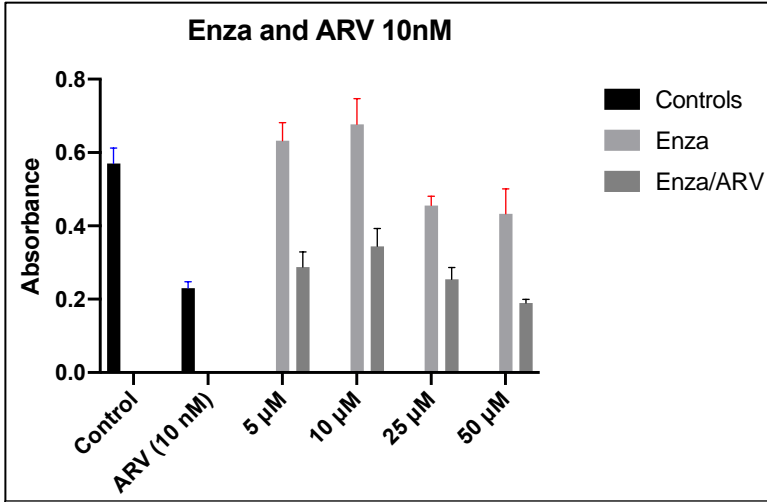
Figure 8A

LNCaP cells were plated in 96 well plates and grown for 48 hours before enzalutamide was added to select wells for 72 hours at day 0. Enzalutamide was removed on day 3 followed by addition of 10 nM ARV-825 to select wells for 96 hours. The doses for enzalutamide were 5, 10, 25, and 50 µM. The MTS assay absorbances were determined using a UV plate reader. Data represent means ± standard errors for three experiments.
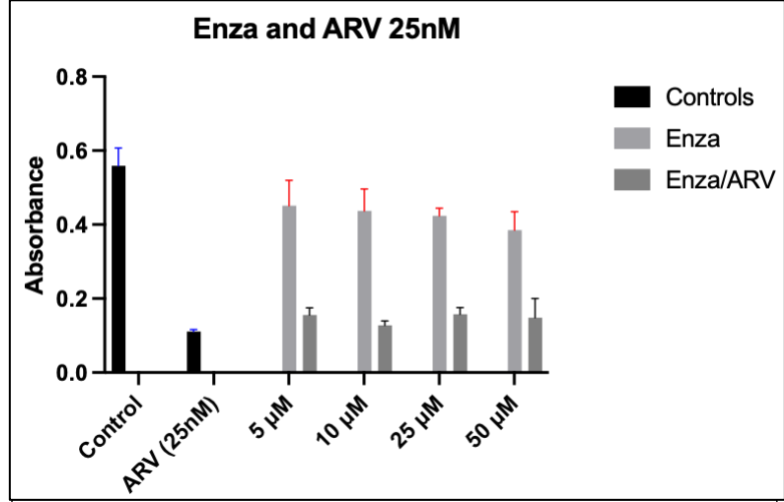
Figure 8B

LNCaP cells were plated in 96 well plates and grown for 48 hours before enzalutamide was added to select wells for 72 hours at day 0. Enzalutamide was removed on day 3 followed by addition of 25 nM ARV-825 to select wells for 96 hours. The doses for enzalutamide were 5, 10, 25, and 50 µM. The MTS assay absorbances were determined using a UV plate reader. Data represent means ± standard errors for three experiments.

Figure 8C

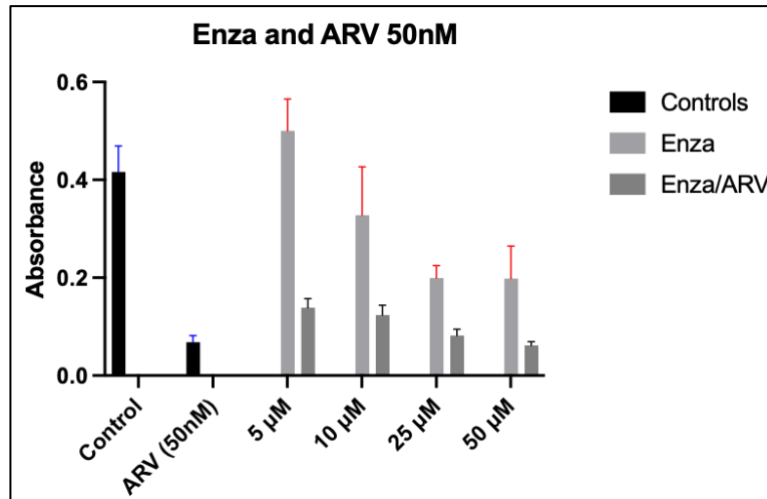LNCaP cells were plated in 96 well plates and grown for 48 hours before enzalutamide was added to select wells for 72 hours at day 0. Enzalutamide was removed on day 3 followed by addition of 50 nM ARV-825 to select wells for 96 hours. The doses for enzalutamide were 5, 10, 25, and 50 µM. The MTS assay absorbances were determined using a UV plate reader. Data represent means ± standard errors for three experiments.
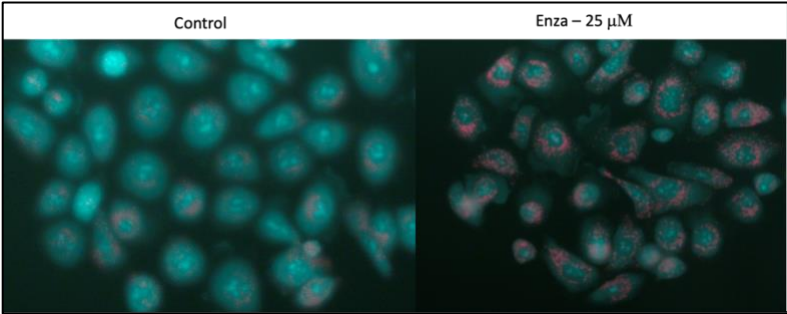
Figure 8D

PC3 cells were treated with 25 μM enzalutamide and stained with acridine orange after 96 hours. The cells were imaged using a fluorescent microscope with all images being taken at the same magnification.
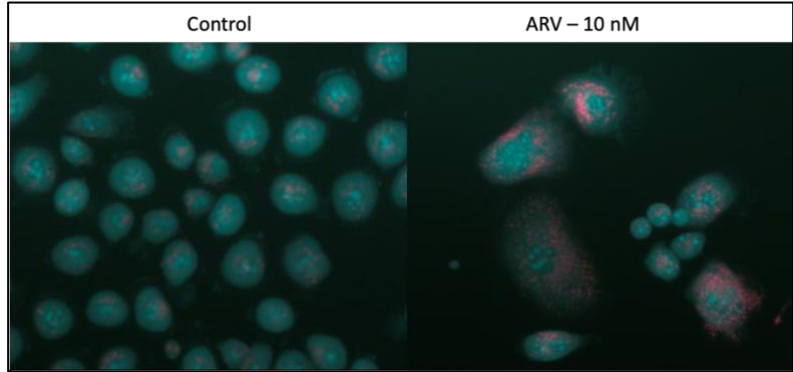
Figure 8E

PC3 cells were treated with 10 nM ARV-825 and stained with acridine orange after 96 hours. The cells were imaged using a fluorescent microscope with all images being taken at the same magnification.

Figure 8F

PC3 cells were treated with 25 nM ARV-825 and stained with acridine orange after 96 hours. The cells were imaged using a fluorescent microscope with all images being taken at the same magnification.

Figure 8G

PC3 cells were treated with 50 nM ARV-825 and stained with acridine orange after 96 hours. The cells were imaged using a fluorescent microscope with all images being taken at the same magnification.

Figure 8H

PC3 cells were treated with 25 μM enzalutamide for 72 hours and then after removal, they were treated with 10 nM ARV-825 for 96 hours and stained with acridine orange after 7 days. The cells were imaged using a fluorescent microscope with all images being taken at the same magnification.

Figure 8I

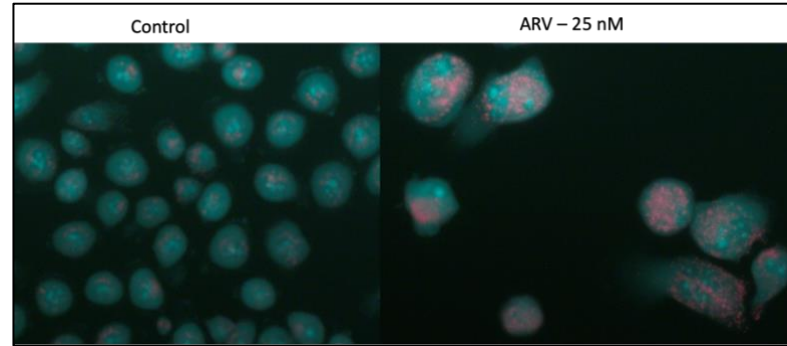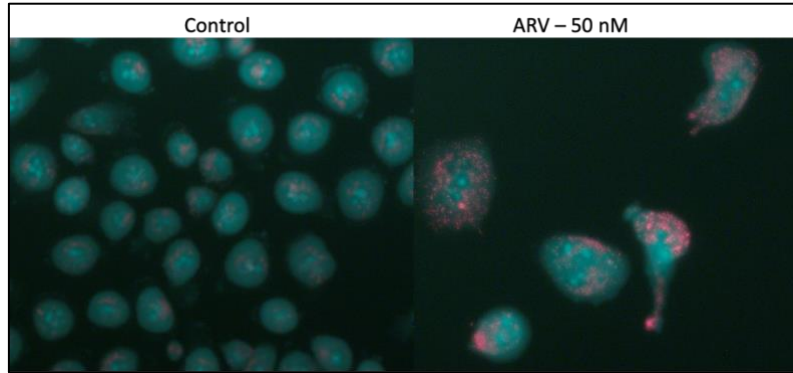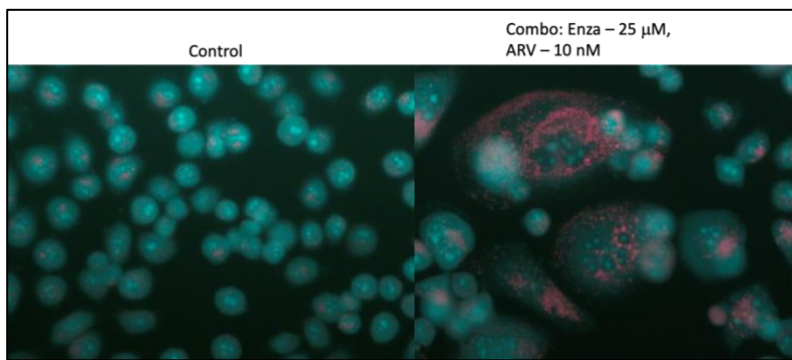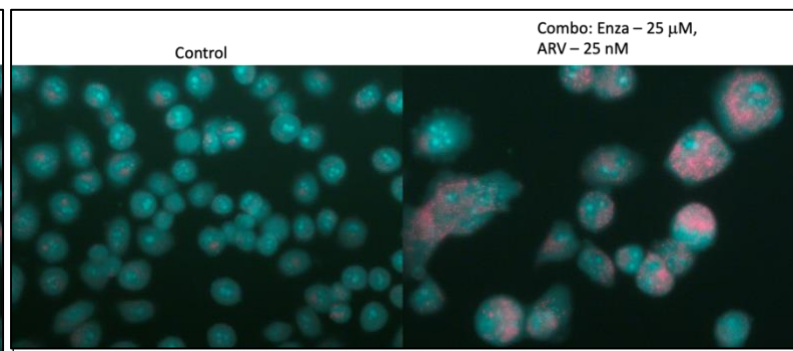PC3 cells were treated with 25 μM enzalutamide for 72 hours and then after removal, they were treated with 25 nM ARV-825 for 96 hours and stained with acridine orange after 7 days. The cells were imaged using a fluorescent microscope with all images being taken at the same magnification.
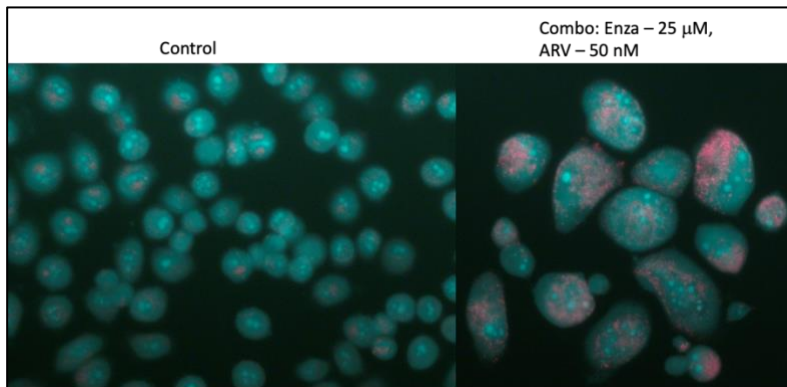
Figure 8J

PC3 cells were treated with 25 μM enzalutamide for 72 hours and then after removal, they were treated with 50 nM ARV-825 for 96 hours and stained with acridine orange after 7 days. The cells were imaged using a fluorescent microscope with all images being taken at the same magnification.
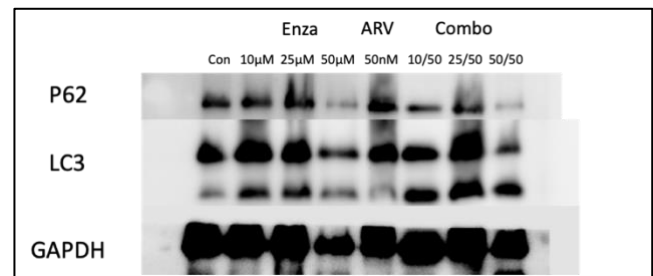
Figure 8K

PC3 cells were treated with either enzalutamide for 72 hours, ARV-825 for 96 hours or both in combination and lysates were collected after the treatments ended. Enzalutamide concentrations were 10, 25 and 50 μM while ARV-825 was 50nM. P62 and LC3 levels were assessed using western blot analysis.

3.2.5. ARV-825 as a monotherapy induces a significant prolonged growth arrest at 100nM in PC3 and DU145 cells

The data in Figures 7 and 8 clearly demonstrated ARV-825 being effective as a monotherapy in a dose dependent manner for both PC3 and LNCaP cell lines. ARV-825 is a BET inhibitor that normally functions as a degrader of BRD4, which is elevated in cancer cells [132], [136]. Furthermore, there are clinical studies that have linked low BRD4 expression with prolongation of prostate cancer patient survival [150]. To interrogate whether ARV-825 is suppressing its putative target, BRD4, as well as to determine the best concentrations to utilize for further experiments with ARV-825 in PC3 cells, a Western Blot analysis was performed using different concentrations of ARV-825 to assess levels of BRD4. Figure 9A shows a reduction in

levels of BRD4 in PC3 cells as the ARV-825 concentration is increased. Similarly, in DU145 cells in Figure 9B, which we decided to bring back as a comparison study here, BRD4 levels decreased in a dose dependent manner as the ARV-825 concentration increased, with the 100nM dose almost fully degrading this target protein. The effects of ARV-825 on c-Myc levels, which has a central role in almost every aspect of the oncogenic process, orchestrating proliferation, apoptosis, differentiation, and metabolism, were also evaluated using the PC3 cells and ARV-825 concentrations in a dose dependent manner. As shown in Figure 9C, downregulation of c-Myc is evident in the PC3 cells treated with ARV-825 as compared to the control, especially at 100nM, which can be indicative of growth arrest and lack of cell proliferation.

The western blot analyses in Figure 9 provided evidence of ARV-825's effectiveness in degrading BRD4, especially at 100nM. Therefore, selecting this 100nM dose for use in a cell viability assay was the next logical step. Figure 10A presents a determination of viable cell number using a time course assay on the indicated days after exposure to 100 nM ARV-825 for 96 hours, where fresh media was replenished after drug removal on day 4, for DU145 and PC3 cells. It is clear from this data that a significant prolonged growth arrest began almost immediately with addition of the drug and was sustained for the duration of the 14 day time course. This effect is not unexpected given the effect of 100 nM on BRD4 levels in Figure 9; nonetheless the fact that the cells did not recover at all in this time indicates that ARV-825 is very effective alone even at a clinically relevant and safe nanomolar dose.

Although recent studies have investigated the possible utilization of BET inhibitors such as ARV-825 as senolytics, it was still important to eliminate whether senescence was involved [133]. Figure 10B shows β-gal staining for DU145 and PC3 cells with a 96 hour treatment of 100 nM of ARV-825 on day 4 as compared to untreated controls. The lack of morphological changes

as well as lack of staining in either of the cell lines confirms that the growth arrest produced by ARV-825 is not due to senescence.

Furthermore, as a complement to the studies presented here, HSLCI was utilized to generate a profile for the mass and area of these cells, which allows for additional evaluation of senescence; senescent cells tend to be larger in size, consistent with the cellular flattening that characterizes the senescence-like phenotype. HSLCI is a label-free technique that measures the phase shift induced in light traveling through a cell to quantify its mass with picogram sensitivity [116], [117]. Both DU145 and PC3 cell lines were treated with 100 nM of ARV-825 for four days and analyzed with HSLCI on day 4 alongside untreated controls that were analyzed on day 0 and day 4 to generate distributions of median cell mass and median cell area. Figure 10C represents the mass and area profiles for the DU145 cells. It's evident that the mass and area decreased from the controls to the treated cells on day 4 but overall, the data is similar and does not indicate senescence in this cell line. On the other hand, the treated PC3 cells in Figure 10D increased in area and mass, which is consistent with the senescence phenotype. However, this difference does not appear to be very significant, especially when also considering the lack of beta-gal staining in these cells in Figure 10B.

While there is strong evidence that the growth arrest produced is not attributed to senescence, evaluation of apoptosis in the PC3 cells would allow us to narrow down further the nature of this growth arrest. Figure 10E shows PC3 cells treated with 100 nM of ARV-825 for 96 hours alongside an untreated control; these cells were stained with Annexin V/PI and then quantified using flow cytometry to get the percentage of apoptosis. Compared to the controls which showed about 5% apoptosis, the ARV-825 treated cells had a minimal increase in apoptosis induction to about 14%, which is not very significant.

Therefore, the nature of the growth arrest effect here is still unknown. There have been studies from this lab that have shown ARV-825 acting as a senostatic in a breast cancer model, though the prostate cancer cells here were not induced into senescence and therefore, this effect would not be occurring [136]. Senostatics are small molecules that suppress senescent phenotypes without killing cells but can induce or prolong growth arrest [50], [53].
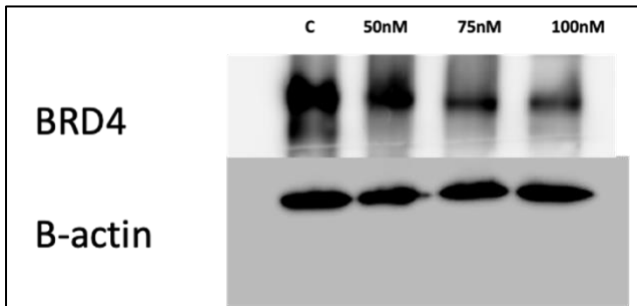
Figure 9A

PC3 cells were treated with ARV-825 for 96 hours and lysates were collected after the treatment ended. ARV-825 concentrations were 50, 75 and 100 nM. BRD4 levels were assessed using western blot analysis.
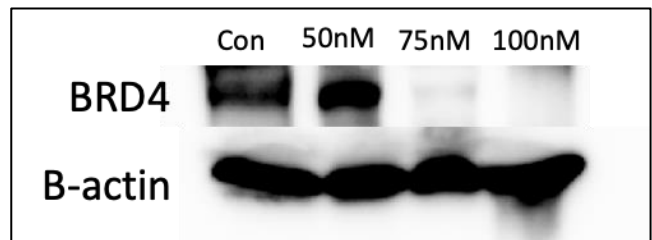
Figure 9B

DU145 cells were treated with ARV-825 for 96 hours and lysates were collected after the treatment ended. ARV-825 concentrations were 50, 75 and 100 nM. BRD4 levels were assessed using western blot analysis.
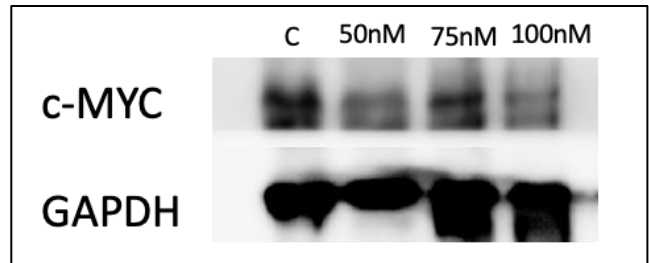
Figure 9C

PC3 cells were treated with ARV-825 for 96 hours and lysates were collected after the treatment ended. ARV-825 concentrations were 50, 75 and 100 nM. C-MYC levels were assessed using western blot analysis.
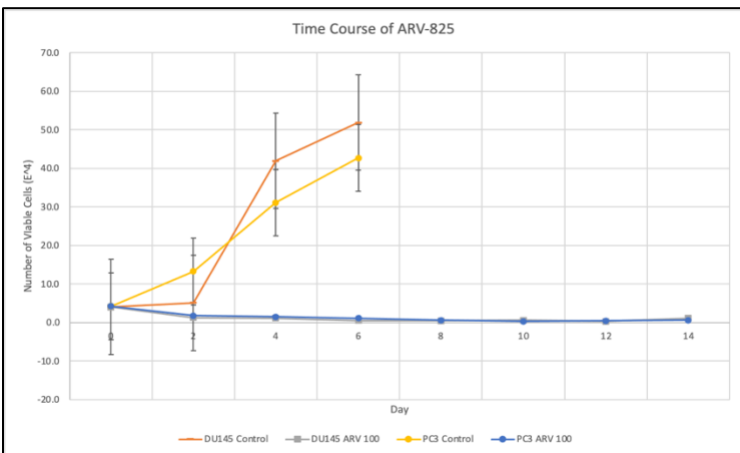
Figure 10A

PC3 and DU145 cells were plated at a 2x10^4 concentration and left to grow for 48 hours before adding ARV-825 at 100 nM concentration to each well on day 0 and the drug was removed on day 4. The cells were counted for each condition every two days until day 14. Data represent means ± standard errors for three experiments.
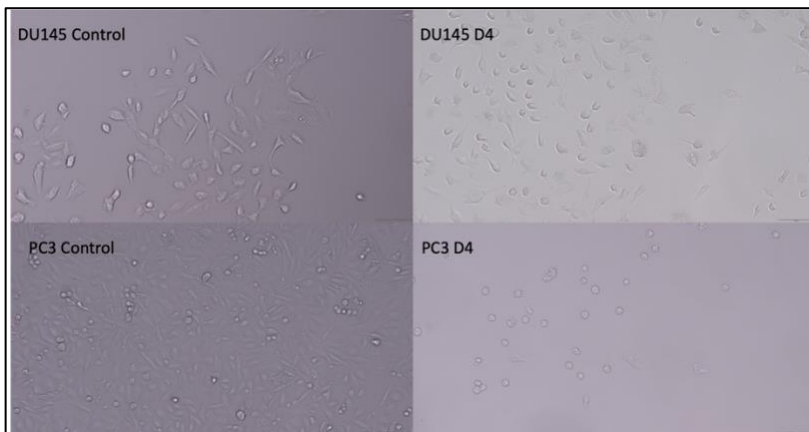
Figure 10B

DU145 and PC3 cells were plated at a 2x10^4 concentration and left to grow for 48 hours before addition of ARV-825 for 96 hours at 100 nM concentration to each plate on day 0. Cells were fixed on day 4, stained with x-gal staining solution and imaged using brightfield microscope. All images were taken at the same magnification.
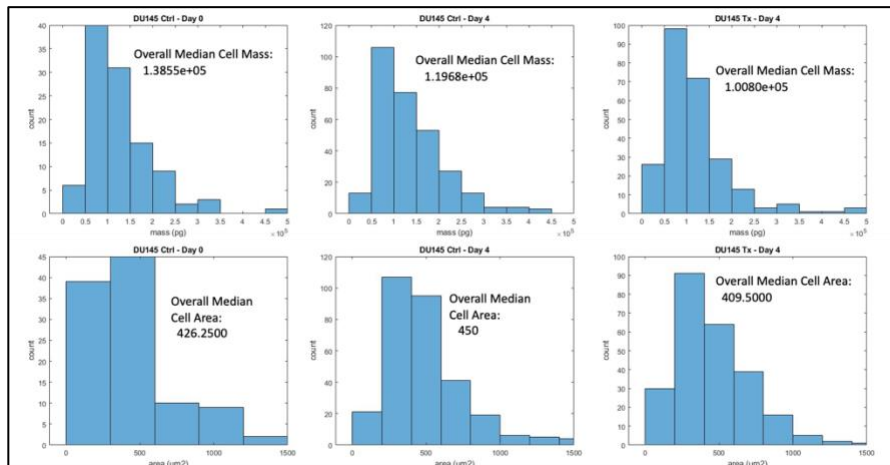
Figure 10C

DU145 cells were plated at a 0.5x10^4 concentration in a 24 well plate and left to grow for 48 hours before addition of ARV-825 for 96 hours at 100 nM concentration to each plate on day 0. Median cell mass and area distribution profiles were generated using HSLCI on the respective days.
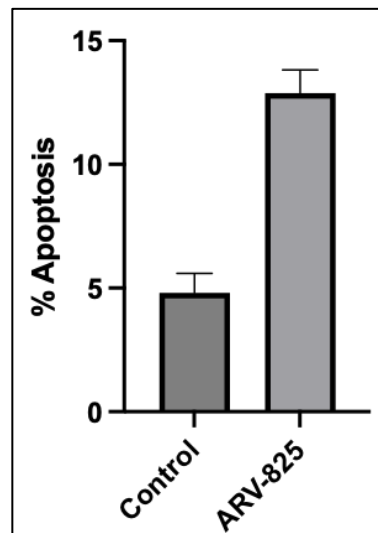
Figure 10E

PC3 cells were treated with ARV-825 for 96 hours at 100 nM concentration while controls were untreated. Apoptosis was measured using Annexin V/PI staining. Staining was performed on day 4 and fluorescence was measured using flow cytometry. Data is from three independent experiments.
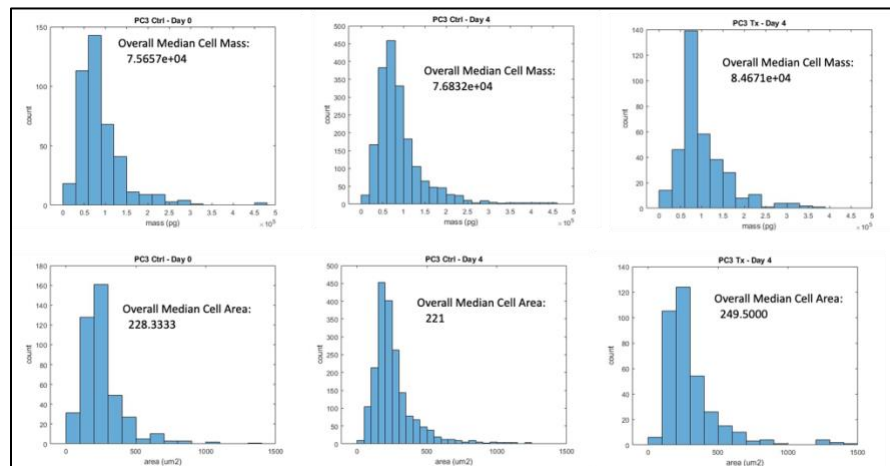
Figure 10D

PC3 cells were plated at a 0.5x10^4 concentration in a 24 well plate and left to grow for 48 hours before addition of ARV-825 for 96 hours at 100 nM concentration to each plate on day 0. Median cell mass and area distribution profiles were generated using HSLCI on the respective days.

3.3. Discussion

Development of castration-resistant prostate cancer and eventual resistance to androgen deprivation therapy leading to disease recurrence is an ongoing issue contributing to the majority of prostate cancer deaths in men. This recurrence can be attributed to a therapy-induced residual dormant tumor cell population that can escape and often become more aggressive in nature [40], [47]. While therapy-induced senescence has been studied for decades, successful utilization of senolytics in cancer treatment has not yet been implemented or approved for clinical use. Despite this, several senolytic agents have been considered and studied to modulate and eliminate senescent tumor cells.

The current work evaluated the standard of care anti-androgen's, enzalutamide and abiraterone, and their ability to induce growth arrest and possibly senescence in androgen-independent cell lines. We initially screened these drugs to determine effective concentrations in the DU145 and PC3 cells. Treatment with enzalutamide and abiraterone at the chosen concentrations produced a transient, growth arrest response; however, these doses are high and are not at clinically relevant concentrations. Furthermore, neither drug induced senescence in DU145 cells while both induced very minimal senescence in the PC3 cells.

Despite these negative results, this did not rule out the possibility that a potential senolytic such as the BET degrader, ARV-825, would be effective in enhancing the response to enzalutamide in PC3 cells; ABT-263 normally works only in senescent cells and so it did not make sense to pursue it further in this case. Screening for ARV-825 in PC3 cells was very promising as the dose-response produced a classic sigmoidal curve. ARV-825 has been used in pre-clinical studies with different cancer types, and we hypothesized that ARV-825 could potentially improve androgen independent CRPC's response to enzalutamide [132], [136]. The

results in the combination studies were somewhat surprising; while the ARV-825 failed to enhance the response to enzalutamide in PC3 cells, it had a significant effect as a monotherapy in these studies. For comparison, ARV-825 also failed to enhance the response to enzalutamide in the androgen-dependent LNCaP cells, though the combination did not render ARV-825 ineffective as was the case in the PC3 cells. This opened two potential new directions: look at ARV-825 as a monotherapy in androgen-independent cells or try to explain the phenomenon occurring in the combination of enzalutamide with ARV-825. Studies were done to try to understand the ineffectiveness of ARV-825 in the combination, though this proved difficult with enzalutamide inducing autophagy being a possible explanation. Future studies such as those with lysosomal protease inhibitors would need to be conducted to confirm whether enzalutamide and/or ARV-825 is responsible for autophagy and whether this is due to cytoprotective autophagy or another functional form of autophagy.

The most promising direction to come from these studies is the possible use of ARV-825 as a monotherapy in androgen-independent cells. ARV-825 as a monotherapy induced a significant prolonged growth arrest at 100nM in PC3 and DU145 cells. The ARV-825 not only had a clear dose-dependent response on BRD4 in both cell lines but also showed downregulation of *c-myc*, especially at a 100nM concentration in PC3 cells. The ARV-825 also did not induce senescence, despite the significant growth arrest. Moreover, the ARV-825 did not induce significant apoptosis either. The nature of this growth arrest remains to be investigated as ARV-825 could prove to be a clinically relevant strategy in the treatment of castration-resistant prostate cancer.

Another possible direction to take this research is the incorporation of a *myc* inhibitor or docetaxel, which is a standard DNA-damaging agent used in CRPC, in combination with

senolytics in androgen independent cells. Preliminary studies showed the effectiveness of docetaxel in PC3 cells alone and in combination with ABT-263 and ARV-825. The apparent synergy of these drugs would be a significant step towards improving current castration-resistant prostate cancer therapy.

There are also Mcl-1 inhibitors that have been proven to be effective in other cancer models [151]. Mcl-1 is an antiapoptotic protein encoded by the gene MCL-1, and is a member of the Bcl-2 family [152]. It has been shown that inhibition of the synthesis of Mcl-1 induces apoptosis and that Mcl-1 is upregulated during senescence [153]. Therefore, the use of an Mcl-1 inhibitor in combination as a senolytic may be useful for treatment of prostate cancer after induction of senescence with a DNA-damaging agent such as docetaxel.

Chapter 4: Supplementary Data

4.1. Introduction

It is important to note that the work in this chapter was the original focus of this research. Based on previous work in this lab as well as other studies in breast cancer, Palbociclib was chosen as a drug to pursue for CRPC, specifically the two androgen independent cell lines, DU145 and PC3 [56], [136], [154]. Palbociclib is a selective inhibitor of the cyclin-dependent kinases CDK4 and CDK6 and has been approved for use in breast cancer [155]. The chosen cell lines are important as DU145 is Rb deficient while PC3 Rb competent, which is very relevant to the mechanism of action of Palbociclib. In the cell cycle, CDK4 and CDK6 complex with cyclin D to drive the phosphorylation of Rb, which allows the cell to pass "R", the restriction point, and commit to division [156]. If Rb is nonfunctional as is the case for DU145 cells, then the growth will be less controlled and the cancer can grow prolifically. Furthermore, in theory, this should make it difficult to inhibit CDK4/6 in this cell line and Palbociclib will not be effective, allowing the DU145 cells to serve as a negative control. The data below was very promising in conjunction with the planned studies with ABT-263 and other senolytics; however, this direction was changed due to a paper that was published in April 2022 that used this same model of Palbociclib with ABT-263 with robust studies that would not have been possible with the resources in our lab [157].

4.2. Results

4.2.1. Palbociclib Produces Growth Arrest in PC3 Cells but Not in DU145 Cells

The CDK 4/6 inhibitor, Palbociclib, has been shown to induce a state of cell cycle growth arrest in several different tumor cell lines [136], [154], [155]. The present studies were performed to determine the influence of Palbociclib on growth and viability in p53 deficient prostate tumor cell lines PC3 and DU145 (also lacks functional Rb). Supplementary Figures 1A and 1B present determination of viable cell number for DU145 and PC3 cells, respectively, using a time course assay on the indicated days after exposure to 1 μM Palbociclib for 6 days, where fresh media was replenished after drug removal on day 6. Although there is some variability in the data, Palbociclib completely halted the growth of the PC3 cells; however, the cells began to recover from the treatment after a period of 8-12 days. On the other hand, the treated DU145 cells showed no evidence of a reduction in cell number when compared with the cell number of untreated cells throughout the time course. This is consistent with the role of Rb in cell cycle progression and previous work in this and other laboratories [136], [156], [157].
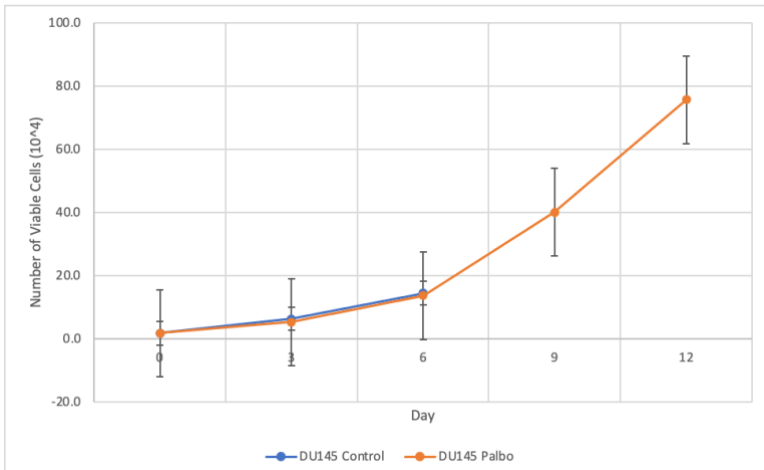
Supplementary Figure 1A

DU145 cells were plated at a 2x10^4 concentration and left to adhere overnight before adding Palbociclib at 1 μM concentration to each well on day 0 to induce growth arrest. Palbociclib was replenished on day 3 before being removed on day 6. The cells were counted for each condition at days 0, 3, 6, 9, and 12. Controls for each cell line were only plated up to D6 due to a high level of confluency after that period. Data represent means ± standard errors for three experiments.
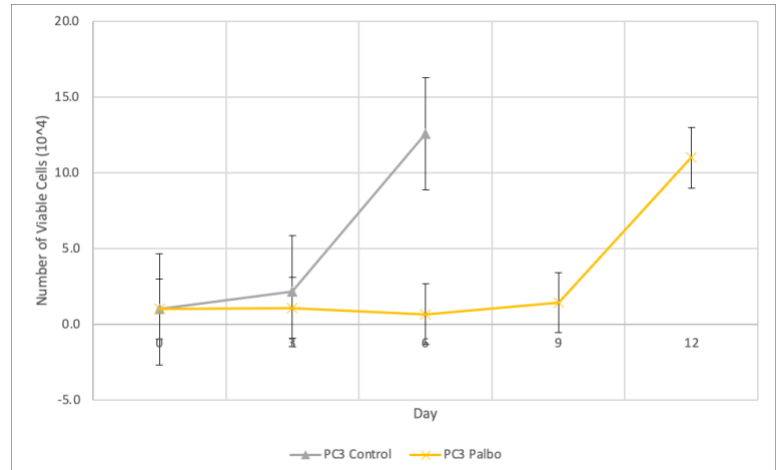
Supplementary Figure 1B

PC3 cells were plated at a 2x10^4 concentration and left to adhere overnight before adding Palbociclib at 1 μM concentration to each well on day 0 to induce growth arrest. Palbociclib was replenished on day 3 before being removed on day 6. The cells were counted for each condition at days 0, 3, 6, 9, and 12. Controls for each cell line were only plated up to D6 due to a high level of confluency after that period. Data represent means ± standard errors for three experiments.

4.2.2. Palbociclib Induces Senescence in PC3 Cells but Not in DU145 Cells

Given that Palbociclib has been shown to promote a transient growth arrest, senescence was examined, which is a durable therapy induced state of growth arrest. Supplementary Figures 2A and 2B demonstrate the promotion of senescence by β-gal staining with a 6 day treatment of 1 μM Palbociclib on the indicated days for PC3 and DU145 cells, respectively, as well as morphological changes (cell enlargement and flattening) associated with senescence. Consistent with the time course results in Figure 1, the PC3 cells showed significant blue-green staining as well as morphological changes for upregulation of β-galactosidase and therefore promotion of senescence, especially at days 6 and 9, whereas the DU145 cells did not have significant staining at any point in the 12 days.
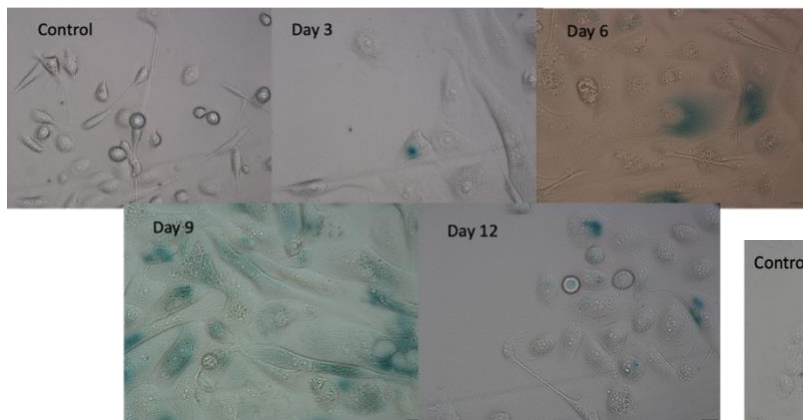
Supplementary Figure 2A

PC3 cells were plated at a 2x10^4 concentration and left to adhere overnight before adding Palbociclib at 1 μM concentration to each plate on day 0 to induce growth arrest. Palbociclib was replenished on day 3 before being removed on day 6. Cells were fixed on each of the indicated days, stained with x-gal staining solution and imaged using brightfield microscope. All images were taken at the same magnification.
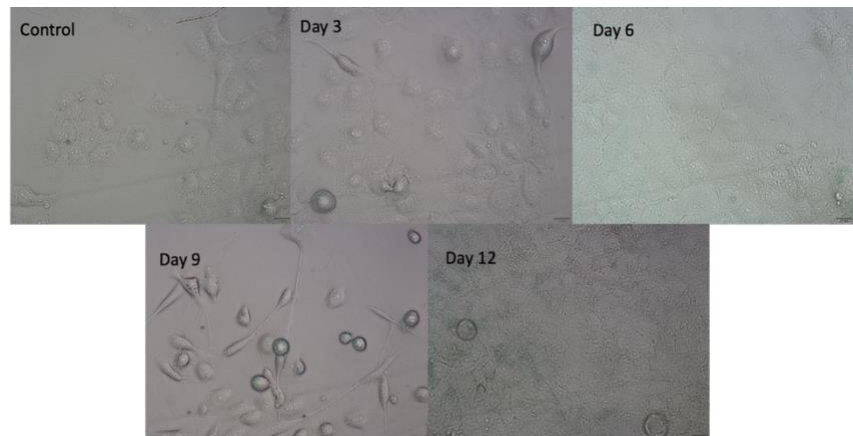
Supplementary Figure 2B

DU145 cells were plated at a 2x10^4 concentration and left to adhere overnight before adding Palbociclib at 1 μM concentration to each plate on day 0 to induce growth arrest. Palbociclib was replenished on day 3 before being removed on day 6. Cells were fixed on each of the indicated days, stained with x-gal staining solution and imaged using brightfield microscope. All images were taken at the same magnification.

4.2.3. ABT-263 Prolongs the Growth Arrest Produced by Palbociclib in PC3 Cells

This laboratory as well as others have demonstrated that the senolytic and BH3 mimetic ABT-263 (navitoclax), is effective at the elimination of tumor cells induced into senescence by various methods in different tumor cell lines [49], [56], [58], [135]. The present studies were performed to determine the influence of ABT-263 alone as well as in combination with Palbociclib on the growth and viability of PC3 prostate cancer cells. Supplementary Figure 3A presents a determination of viable cell number using a time course assay on the indicated days after exposure to 2 μM ABT-263 on day 6, which is the likely peak of senescence, for 48 hours, where fresh media was replenished on day 8. Supplementary Figure 3B shows the viable cell number after exposure to 1 μM Palbociclib for 6 days followed by removal of Palbociclib and addition of 2 μM ABT-263 on day 6 for 48 hours followed by fresh media on day 8. This sequential combination was compared to the 6 day treatment of 1 μM Palbociclib alone in Supplementary Figure 3B. The data in Supplementary Figure 3A demonstrates no evidence of growth arrest and is consistent with previous work in that ABT-263 would only be effective in cells already induced into senescence [49], [56], [120]. In contrast, Supplementary Figure 3B shows evidence of a continuation of the growth delay already seen in Palbociclib alone in PC3 cells when ABT-263 is added sequentially.
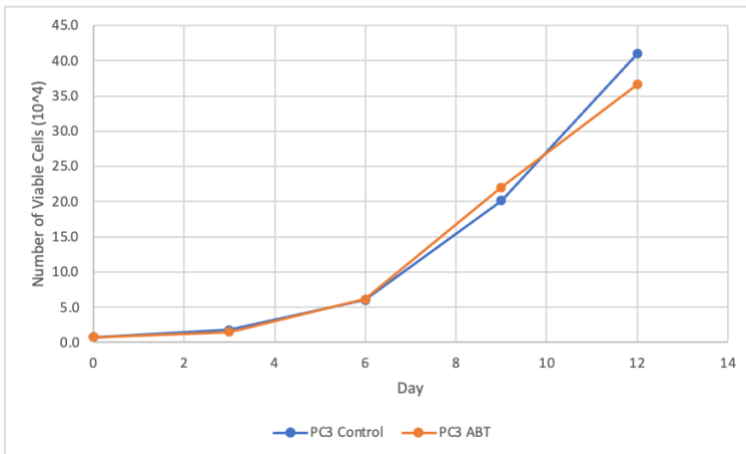
Supplementary Figure 3A

PC3 cells were plated at a 0.5x10^4 concentration with half the wells with controls and half the wells with ABT only. ABT-263 was added to the ABT only wells at 2 µM concentration at day 6 for 48 hours and removed on day 8. The cells were counted for each condition at days 0, 3, 6, 9, and 12.
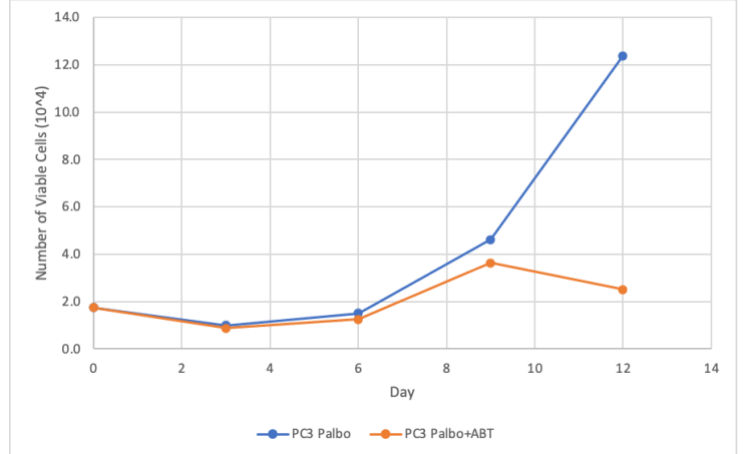
Supplementary Figure 3B

PC3 cells were plated at a 2x10^4 concentration with some wells indicating Palbociclib only and others indicating Palbociclib plus ABT-263 and left to adhere overnight before adding Palbociclib at 1 µM concentration to each well on day 0 to induce senescence. Palbociclib was replenished on day 3 before being removed on day 6. ABT-263 was added to the wells indicating Palbociclib plus ABT-263 at 2 µM concentration at day 6 for 48 hours and removed on day 8. The cells were counted for each condition at days 0, 3, 6, 9, and 12.

4.2.4. Potential senolytic combinations with docetaxel in androgen-independent PC3 cells show promise for future studies

In CRPC, traditional standard of care treatment involves a combination of androgen deprivation with enzalutamide and docetaxel [15], [21], [24], [120]. Given that CRPC can be androgen independent like the PC3 and DU145 cell lines, androgen deprivation should not have any effect. Similarly, enzalutamide relies on the androgen receptor and should also not have any effect on it's own at a normal human blood circulating concentration; in this case 10 µM falls within that range and is regularly used *in vitro* [120], [141]. On the other hand, docetaxel is a DNA damaging agent and should have an effect and induce senescence; in these experiments, 3 nM docetaxel was used as it falls within the range of human blood circulating concentration [158]. Senolytics such as ABT-263 target cells in senescence and therefore, it is predicted that if PC3 cells are induced into senescence by docetaxel, they can be targeted by senolytics to produce an even greater effect than either drug alone.

Supplementary Figure 4A shows the effects of standard of care treatment in PC3 cells and was generated using an MTS assay. Enzalutamide, charcoal-stripped media (CS) for androgen deprivation and docetaxel were used to treat the cells for 72 hours, or 3 days. Each of the 3 conditions were given alone as well as enzalutamide in combination with each of CS and docetaxel. As expected, only docetaxel had a significant effect on the PC3 cells; enzalutamide in combination with docetaxel had the same effect though enzalutamide alone did not have any effect, which means that any effect from that combination is attributed solely to the docetaxel.

Supplementary Figures 4B and 4C represent these standard of care combinations of enzalutamide with docetaxel or CS followed by either ABT-263 or ARV-825 in sequence, respectively. Note that continuous CS means that ABT-263 or ARV-825 were combined with CS media instead of regular media after the 3 days of the standard treatments. ABT-263 was added for 48 hours at 2 μM while ARV-825 was added for 96 hours at 50 nM. Supplementary Figure 4B showing the ABT-263 combination reveals a significant effect only with the docetaxel; this is not surprising as CS has no effect in these cells and ABT-263 is not known to be effective if cells are not induced into senescence. Conversely, in Supplementary Figure 4C, ARV-825 shows some effects in the CS combination though this is due to ARV-825's effects alone and not the CS media. However, the combination of ARV-825 with docetaxel is very significant and it appears that the cells are almost depleted from the synergy of the two drugs.

In cancer, *Myc* genes are upregulated and are involved in cell proliferation [159]. Therefore, drugs that inhibit c-*myc* should follow sensibly and reduce proliferation. Here, a dose-response curve was generated in Supplementary Figure 4D for the *myc* inhibitor drug, 10058-F4, in a range of 0 to 125 μM for 96 hours. From this curve, it would be useful to test both 25 and 50 μM concentrations in combination with standard of care treatments as those doses appear to be

the lowest doses that have an effect in PC3 cells. Based on the apparent effectiveness of the *myc* inhibitor in these preliminary studies in PC3 cells as well as docetaxel's very significant effects alone or in combination with various senolytics, testing combinations of docetaxel with a *myc* inhibitor shows substantial promise for future studies in castration resistant prostate cancer.

3 Day Combo
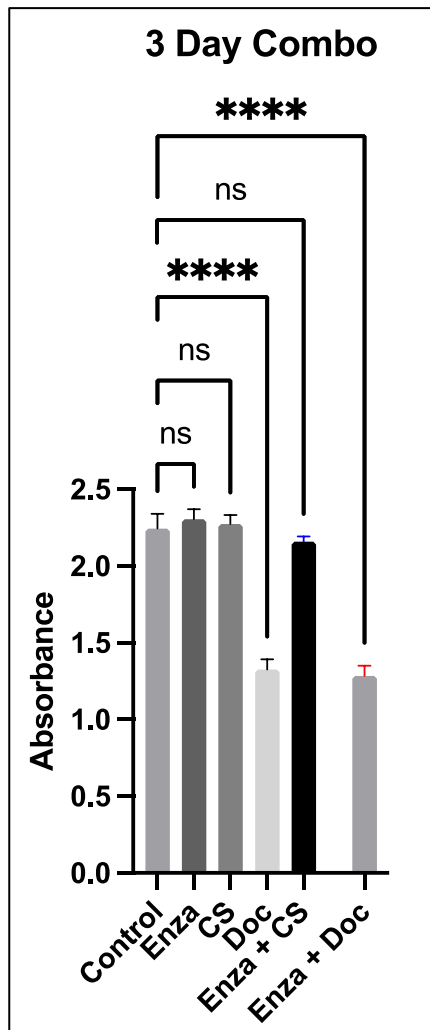
Supplementary Figure 4A

PC3 cells were plated in 96 well plates and allowed to adhere overnight before enzalutamide (10 μM), charcoal-stripped media (CS), docetaxel (3 nM), or combinations of these were added to select wells for 72 hours at day 0. The MTS assay absorbances were determined using a UV plate reader. Data represent means ± standard errors for six experiments.

5 Day Combo
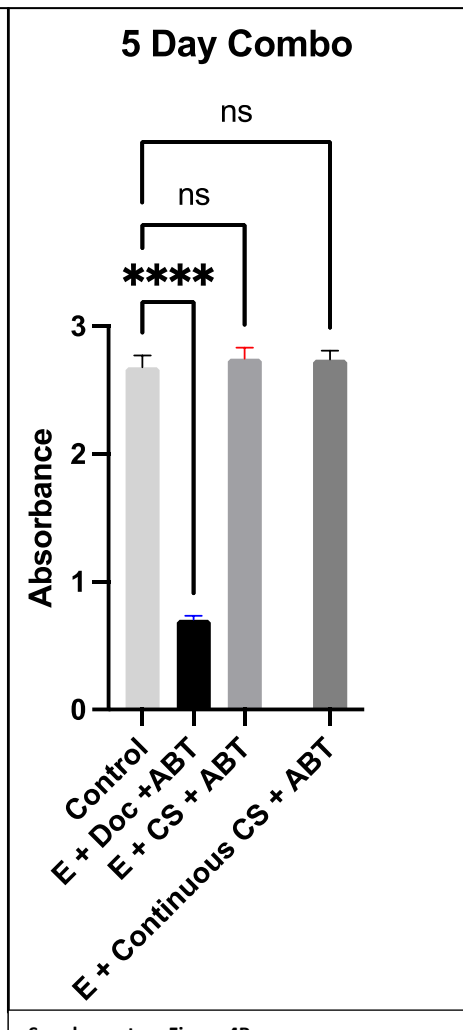
Supplementary Figure 4B

PC3 cells were plated in 96 well plates and allowed to adhere overnight before combinations of enzalutamide (10 μM), charcoal-stripped media (CS) and docetaxel (3 nM) were added to select wells for 72 hours at day 0. After 72 hours, these drugs were removed and ABT-263 (2 μM) was added for 48 hours. The MTS assay absorbances were determined using a UV plate reader. Data represent means ± standard errors for six experiments.

7 Day Combo
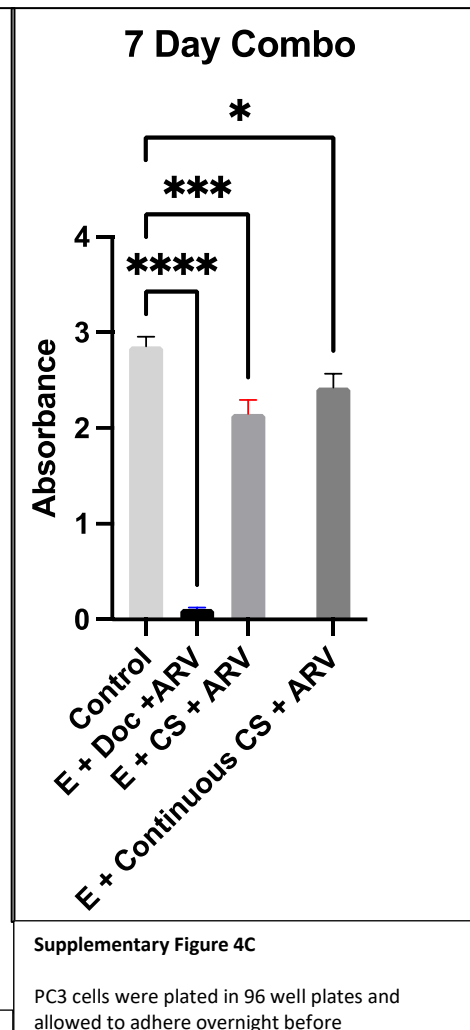
Supplementary Figure 4C

PC3 cells were plated in 96 well plates and allowed to adhere overnight before combinations of enzalutamide (10 μM), charcoal-stripped media (CS) and docetaxel (3 nM) were added to select wells for 72 hours at day 0. After 72 hours, these drugs were removed and ARV-825 (50 nM) was added for 96 hours. The MTS assay absorbances were determined using a UV plate reader. Data represent means ± standard errors for six experiments.

Myc Inhibitor DR Curve
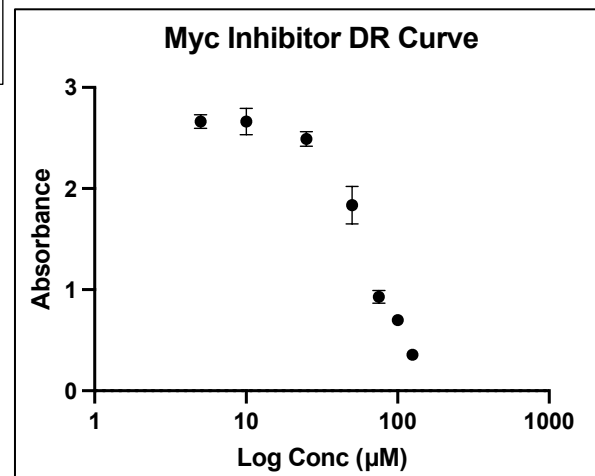
Supplementary Figure 4D

PC3 cells were plated in 96 well plates and treated with the *Myc* inhibitor, 10058-F4, for 96 hours after being left overnight to adhere. The MTS assay was observed in a dose range of 0 to 125 μM and absorbances were determined using a UV plate reader. Data represent means ± standard errors for six experiments.

References

[1]   R. L. Siegel, K. D. Miller, N. S. Wagle, and A. Jemal, "Cancer statistics, 2023," *CA Cancer J Clin*, vol. 73, no. 1, pp. 17–48, Jan. 2023, doi: 10.3322/caac.21763.

[2]   A. Munjal and S. W. Leslie, *Gleason Score*. 2023.

[3]   S. W. Leslie, T. L. Soon-Sutton, A. R I, H. Sajjad, and L. E. Siref, *Prostate Cancer*. 2023.

[4]   A. J. Chang, K. A. Autio, M. Roach, and H. I. Scher, "High-risk prostate cancer—classification and therapy," *Nat Rev Clin Oncol*, vol. 11, no. 6, pp. 308–323, Jun. 2014, doi: 10.1038/nrclinonc.2014.68.

[5]   A. Figueiredo, L. Costa, M. J. Maurício, L. Figueira, R. Ramos, and C. Martins-da-Silva, "Nonmetastatic Castration-Resistant Prostate Cancer: Current Challenges and Trends," *Clin Drug Investig*, vol. 42, no. 8, pp. 631–642, Aug. 2022, doi: 10.1007/s40261-022-01178-y.

[6]   W. P. Harris, E. A. Mostaghel, P. S. Nelson, and B. Montgomery, "Androgen deprivation therapy: progress in understanding mechanisms of resistance and optimizing androgen depletion.," *Nat Clin Pract Urol*, vol. 6, no. 2, pp. 76–85, Feb. 2009, doi: 10.1038/ncpuro1296.

[7]   F. Crowley, M. Sterpi, C. Buckley, L. Margetich, S. Handa, and Z. Dovey, "A Review of the Pathophysiological Mechanisms Underlying Castration-resistant Prostate Cancer," *Res Rep Urol*, vol. Volume 13, pp. 457–472, Jun. 2021, doi: 10.2147/RRU.S264722.

[8]   T. Chandrasekar, J. C. Yang, A. C. Gao, and C. P. Evans, "Targeting molecular resistance in castration-resistant prostate cancer," *BMC Med*, vol. 13, no. 1, p. 206, Dec. 2015, doi: 10.1186/s12916-015-0457-6.

[9]   T. Karantanos, C. P. Evans, B. Tombal, T. C. Thompson, R. Montironi, and W. B. Isaacs, "Understanding the Mechanisms of Androgen Deprivation Resistance in Prostate Cancer at the Molecular Level," *Eur Urol*, vol. 67, no. 3, pp. 470–479, Mar. 2015, doi: 10.1016/j.eururo.2014.09.049.

[10]   M. Y. Teo, D. E. Rathkopf, and P. Kantoff, "Treatment of Advanced Prostate Cancer," *Annu Rev Med*, vol. 70, no. 1, pp. 479–499, Jan. 2019, doi: 10.1146/annurev-med-051517-011947.

[11]   K. Fizazi *et al.*, "Nonmetastatic, Castration-Resistant Prostate Cancer and Survival with Darolutamide," *New England Journal of Medicine*, vol. 383, no. 11, pp. 1040–1049, Sep. 2020, doi: 10.1056/NEJMoa2001342.

[12]   C. Tran *et al.*, "Development of a second-generation antiandrogen for treatment of advanced prostate cancer.," *Science*, vol. 324, no. 5928, pp. 787–90, May 2009, doi: 10.1126/science.1168175.

[13]   D. P. Petrylak *et al.*, "Docetaxel and Estramustine Compared with Mitoxantrone and Prednisone for Advanced Refractory Prostate Cancer," *New England Journal of Medicine*, vol. 351, no. 15, pp. 1513–1520, Oct. 2004, doi: 10.1056/NEJMoa041318.

[14]   I. F. Tannock *et al.*, "Docetaxel plus Prednisone or Mitoxantrone plus Prednisone for Advanced Prostate Cancer," *New England Journal of Medicine*, vol. 351, no. 15, pp. 1502–1512, Oct. 2004, doi: 10.1056/NEJMoa040720.

[15] K. PIENTA, "Preclinical mechanisms of action of docetaxel and docetaxel combinations in prostate cancer," *Semin Oncol*, vol. 28, pp. 3–7, Aug. 2001, doi: 10.1016/S0093-7754(01)90148-4.

[16] J. S. de Bono *et al.*, "Prednisone plus cabazitaxel or mitoxantrone for metastatic castration-resistant prostate cancer progressing after docetaxel treatment: a randomised open-label trial," *The Lancet*, vol. 376, no. 9747, pp. 1147–1154, Oct. 2010, doi: 10.1016/S0140-6736(10)61389-X.

[17] K. Fizazi *et al.*, "Abiraterone plus Prednisone in Metastatic, Castration-Sensitive Prostate Cancer," *New England Journal of Medicine*, vol. 377, no. 4, pp. 352–360, Jul. 2017, doi: 10.1056/NEJMoa1704174.

[18] G. Attard *et al.*, "Phase I Clinical Trial of a Selective Inhibitor of CYP17, Abiraterone Acetate, Confirms That Castration-Resistant Prostate Cancer Commonly Remains Hormone Driven," *Journal of Clinical Oncology*, vol. 26, no. 28, pp. 4563–4571, Oct. 2008, doi: 10.1200/JCO.2007.15.9749.

[19] J. S. de Bono *et al.*, "Abiraterone and Increased Survival in Metastatic Prostate Cancer," *New England Journal of Medicine*, vol. 364, no. 21, pp. 1995–2005, May 2011, doi: 10.1056/NEJMoa1014618.

[20] C. J. Ryan *et al.*, "Abiraterone in Metastatic Prostate Cancer without Previous Chemotherapy," *New England Journal of Medicine*, vol. 368, no. 2, pp. 138–148, Jan. 2013, doi: 10.1056/NEJMoa1209096.

[21] T. M. Beer *et al.*, "Enzalutamide in Metastatic Prostate Cancer before Chemotherapy," *New England Journal of Medicine*, vol. 371, no. 5, pp. 424–433, Jul. 2014, doi: 10.1056/NEJMoa1405095.

[22] H. I. Scher *et al.*, "Increased Survival with Enzalutamide in Prostate Cancer after Chemotherapy," *New England Journal of Medicine*, vol. 367, no. 13, pp. 1187–1197, Sep. 2012, doi: 10.1056/NEJMoa1207506.

[23] O. Sartor *et al.*, "Samarium-153-Lexidronam complex for treatment of painful bone metastases in hormone-refractory prostate cancer," *Urology*, vol. 63, no. 5, pp. 940–945, May 2004, doi: 10.1016/j.urology.2004.01.034.

[24] N. D. James *et al.*, "Clinical Outcomes and Survival Following Treatment of Metastatic Castrate-Refractory Prostate Cancer With Docetaxel Alone or With Strontium-89, Zoledronic Acid, or Both," *JAMA Oncol*, vol. 2, no. 4, p. 493, Apr. 2016, doi: 10.1001/jamaoncol.2015.5570.

[25] C. Parker *et al.*, "Alpha Emitter Radium-223 and Survival in Metastatic Prostate Cancer," *New England Journal of Medicine*, vol. 369, no. 3, pp. 213–223, Jul. 2013, doi: 10.1056/NEJMoa1213755.

[26] E. J. Small *et al.*, "Placebo-Controlled Phase III Trial of Immunologic Therapy with Sipuleucel-T (APC8015) in Patients with Metastatic, Asymptomatic Hormone Refractory Prostate Cancer," *Journal of Clinical Oncology*, vol. 24, no. 19, pp. 3089–3094, Jul. 2006, doi: 10.1200/JCO.2005.04.5252.

[27] C. C. Pritchard *et al.*, "Inherited DNA-Repair Gene Mutations in Men with Metastatic Prostate Cancer," *New England Journal of Medicine*, vol. 375, no. 5, pp. 443–453, Aug. 2016, doi: 10.1056/NEJMoa1603144.

[28] J. Mateo *et al.*, "DNA-Repair Defects and Olaparib in Metastatic Prostate Cancer," *New England Journal of Medicine*, vol. 373, no. 18, pp. 1697–1708, Oct. 2015, doi: 10.1056/NEJMoa1506859.

[29] D. T. Le *et al.*, "Mismatch repair deficiency predicts response of solid tumors to PD-1 blockade," *Science (1979)*, vol. 357, no. 6349, pp. 409–413, Jul. 2017, doi: 10.1126/science.aan6733.

[30] W. Abida *et al.*, "Microsatellite instability in prostate cancer and response to immune checkpoint blockade.," *Journal of Clinical Oncology*, vol. 36, no. 15_suppl, pp. 5020–5020, May 2018, doi: 10.1200/JCO.2018.36.15_suppl.5020.

[31] C. C. Pritchard *et al.*, "Complex MSH2 and MSH6 mutations in hypermutated microsatellite unstable advanced prostate cancer," *Nat Commun*, vol. 5, no. 1, p. 4988, Sep. 2014, doi: 10.1038/ncomms5988.

[32] L. Hayflick and P. S. Moorhead, "The serial cultivation of human diploid cell strains," *Exp Cell Res*, vol. 25, no. 3, pp. 585–621, Dec. 1961, doi: 10.1016/0014-4827(61)90192-6.

[33] N. E. Sharpless and C. J. Sherr, "Forging a signature of in vivo senescence.," *Nat Rev Cancer*, vol. 15, no. 7, pp. 397–408, Jul. 2015, doi: 10.1038/nrc3960.

[34] A. Hernandez-Segura, J. Nehme, and M. Demaria, "Hallmarks of Cellular Senescence.," *Trends Cell Biol*, vol. 28, no. 6, pp. 436–453, Jun. 2018, doi: 10.1016/j.tcb.2018.02.001.

[35] B. G. Childs, M. Durik, D. J. Baker, and J. M. van Deursen, "Cellular senescence in aging and age-related disease: from mechanisms to therapy," *Nat Med*, vol. 21, no. 12, pp. 1424–1435, Dec. 2015, doi: 10.1038/nm.4000.

[36] J. Campisi, "Cellular senescence as a tumor-suppressor mechanism," *Trends Cell Biol*, vol. 11, no. 11, pp. S27–S31, Nov. 2001, doi: 10.1016/S0962-8924(01)02151-1.

[37] P. Hinds and J. Pietruska, "Senescence and tumor suppression.," *F1000Res*, vol. 6, p. 2121, 2017, doi: 10.12688/f1000research.11671.1.

[38] M. Collado *et al.*, "Senescence in premalignant tumours," *Nature*, vol. 436, no. 7051, pp. 642–642, Aug. 2005, doi: 10.1038/436642a.

[39] Y. Stroikin, H. Dalen, U. T. Brunk, and A. Terman, "Testing the 'garbage' accumulation theory of ageing: mitotic activity protects cells from death induced by inhibition of autophagy.," *Biogerontology*, vol. 6, no. 1, pp. 39–47, 2005, doi: 10.1007/s10522-004-7382-y.

[40] T. Saleh *et al.*, "Therapy-Induced Senescence: An 'Old' Friend Becomes the Enemy," *Cancers (Basel)*, vol. 12, no. 4, p. 822, Mar. 2020, doi: 10.3390/cancers12040822.

[41] S. Dodig, I. Čepelak, and I. Pavić, "Hallmarks of senescence and aging.," *Biochem Med (Zagreb)*, vol. 29, no. 3, p. 030501, Oct. 2019, doi: 10.11613/BM.2019.030501.

[42] J. M. Vicencio *et al.*, "Senescence, apoptosis or autophagy? When a damaged cell must decide its path--a mini-review.," *Gerontology*, vol. 54, no. 2, pp. 92–9, 2008, doi: 10.1159/000129697.

[43] S. Yanagi, H. Tsubouchi, A. Miura, A. Matsuo, N. Matsumoto, and M. Nakazato, "The Impacts of Cellular Senescence in Elderly Pneumonia and in Age-Related Lung Diseases That Increase the Risk of Respiratory Infections.," *Int J Mol Sci*, vol. 18, no. 3, Feb. 2017, doi: 10.3390/ijms18030503.

[44]   S. Özcan *et al.*, "Unbiased analysis of senescence associated secretory phenotype (SASP) to identify common components following different genotoxic stresses.," *Aging*, vol. 8, no. 7, pp. 1316–29, Jul. 2016, doi: 10.18632/aging.100971.

[45]   S. Watanabe, S. Kawamoto, N. Ohtani, and E. Hara, "Impact of senescence-associated secretory phenotype and its potential as a therapeutic target for senescence-associated diseases.," *Cancer Sci*, vol. 108, no. 4, pp. 563–569, Apr. 2017, doi: 10.1111/cas.13184.

[46]   E. González-Gualda, A. G. Baker, L. Fruk, and D. Muñoz-Espín, "A guide to assessing cellular senescence in vitro and in vivo.," *FEBS J*, vol. 288, no. 1, pp. 56–80, Jan. 2021, doi: 10.1111/febs.15570.

[47]   D. A. Gewirtz, S. E. Holt, and L. W. Elmore, "Accelerated senescence: an emerging role in tumor cell response to chemotherapy and radiation.," *Biochem Pharmacol*, vol. 76, no. 8, pp. 947–57, Oct. 2008, doi: 10.1016/j.bcp.2008.06.024.

[48]   Y. Sun, J.-P. Coppé, and E. W.-F. Lam, "Cellular Senescence: The Sought or the Unwanted?," *Trends Mol Med*, vol. 24, no. 10, pp. 871–885, Oct. 2018, doi: 10.1016/j.molmed.2018.08.002.

[49]   T. Saleh *et al.*, "Clearance of therapy-induced senescent tumor cells by the senolytic ABT-263 via interference with BCL-XL -BAX interaction.," *Mol Oncol*, vol. 14, no. 10, pp. 2504–2519, Oct. 2020, doi: 10.1002/1878-0261.12761.

[50]   C. Kang, "Senolytics and Senostatics: A Two-Pronged Approach to Target Cellular Senescence for Delaying Aging and Age-Related Diseases.," *Mol Cells*, vol. 42, no. 12, pp. 821–827, Dec. 2019, doi: 10.14348/molcells.2019.0298.

[51]   V. J. Carpenter, T. Saleh, and D. A. Gewirtz, "Senolytics for Cancer Therapy: Is All That Glitters Really Gold?," *Cancers (Basel)*, vol. 13, no. 4, Feb. 2021, doi: 10.3390/cancers13040723.

[52]   S. Short, E. Fielder, S. Miwa, and T. von Zglinicki, "Senolytics and senostatics as adjuvant tumour therapy.," *EBioMedicine*, vol. 41, pp. 683–692, Mar. 2019, doi: 10.1016/j.ebiom.2019.01.056.

[53]   G. Nelson, O. Kucheryavenko, J. Wordsworth, and T. von Zglinicki, "The senescent bystander effect is caused by ROS-activated NF-κB signalling.," *Mech Ageing Dev*, vol. 170, pp. 30–36, Mar. 2018, doi: 10.1016/j.mad.2017.08.005.

[54]   L. Zhang, L. E. Pitcher, V. Prahalad, L. J. Niedernhofer, and P. D. Robbins, "Targeting cellular senescence with senotherapeutics: senolytics and senomorphics," *FEBS J*, vol. 290, no. 5, pp. 1362–1383, Mar. 2023, doi: 10.1111/febs.16350.

[55]   F. Ahmadinejad *et al.*, "Senolytic-Mediated Elimination of Head and Neck Tumor Cells Induced Into Senescence by Cisplatin.," *Mol Pharmacol*, vol. 101, no. 3, pp. 168–180, Mar. 2022, doi: 10.1124/molpharm.121.000354.

[56]   V. Carpenter *et al.*, "Androgen-deprivation induced senescence in prostate cancer cells is permissive for the development of castration-resistance but susceptible to senolytic therapy.," *Biochem Pharmacol*, vol. 193, p. 114765, Nov. 2021, doi: 10.1016/j.bcp.2021.114765.

[57]   N. N. Mohamad Anuar, N. S. Nor Hisam, S. L. Liew, and A. Ugusman, "Clinical Review: Navitoclax as a Pro-Apoptotic and Anti-Fibrotic Agent.," *Front Pharmacol*, vol. 11, p. 564108, 2020, doi: 10.3389/fphar.2020.564108.

[58] D. Mérino *et al.*, "Bcl-2, Bcl-x(L), and Bcl-w are not equivalent targets of ABT-737 and navitoclax (ABT-263) in lymphoid and leukemic cells.," *Blood*, vol. 119, no. 24, pp. 5807–16, Jun. 2012, doi: 10.1182/blood-2011-12-400929.

[59] K. R. Parzych and D. J. Klionsky, "An overview of autophagy: morphology, mechanism, and regulation.," *Antioxid Redox Signal*, vol. 20, no. 3, pp. 460–73, Jan. 2014, doi: 10.1089/ars.2013.5371.

[60] Z. Yang and D. J. Klionsky, "Mammalian autophagy: core molecular machinery and signaling regulation.," *Curr Opin Cell Biol*, vol. 22, no. 2, pp. 124–31, Apr. 2010, doi: 10.1016/j.ceb.2009.11.014.

[61] D. Mijaljica, M. Prescott, and R. J. Devenish, "Microautophagy in mammalian cells: revisiting a 40-year-old conundrum.," *Autophagy*, vol. 7, no. 7, pp. 673–82, Jul. 2011, doi: 10.4161/auto.7.7.14733.

[62] A. Massey, R. Kiffin, and A. M. Cuervo, "Pathophysiology of chaperone-mediated autophagy.," *Int J Biochem Cell Biol*, vol. 36, no. 12, pp. 2420–34, Dec. 2004, doi: 10.1016/j.biocel.2004.04.010.

[63] T. Yorimitsu and D. J. Klionsky, "Autophagy: molecular machinery for self-eating.," *Cell Death Differ*, vol. 12 Suppl 2, no. Suppl 2, pp. 1542–52, Nov. 2005, doi: 10.1038/sj.cdd.4401765.

[64] C. K. Das, M. Mandal, and D. Kögel, "Pro-survival autophagy and cancer cell resistance to therapy.," *Cancer Metastasis Rev*, vol. 37, no. 4, pp. 749–766, Dec. 2018, doi: 10.1007/s10555-018-9727-z.

[65] L. Poillet-Perez, G. Despouy, R. Delage-Mourroux, and M. Boyer-Guittaut, "Interplay between ROS and autophagy in cancer cells, from tumor initiation to cancer therapy.," *Redox Biol*, vol. 4, pp. 184–92, 2015, doi: 10.1016/j.redox.2014.12.003.

[66] J. Kim, M. Kundu, B. Viollet, and K.-L. Guan, "AMPK and mTOR regulate autophagy through direct phosphorylation of Ulk1.," *Nat Cell Biol*, vol. 13, no. 2, pp. 132–41, Feb. 2011, doi: 10.1038/ncb2152.

[67] I. Dikic and Z. Elazar, "Mechanism and medical implications of mammalian autophagy.," *Nat Rev Mol Cell Biol*, vol. 19, no. 6, pp. 349–364, Jun. 2018, doi: 10.1038/s41580-018-0003-4.

[68] P. Ylä-Anttila, H. Vihinen, E. Jokitalo, and E.-L. Eskelinen, "3D tomography reveals connections between the phagophore and endoplasmic reticulum.," *Autophagy*, vol. 5, no. 8, pp. 1180–5, Nov. 2009, doi: 10.4161/auto.5.8.10274.

[69] D. W. Hailey *et al.*, "Mitochondria supply membranes for autophagosome biogenesis during starvation.," *Cell*, vol. 141, no. 4, pp. 656–67, May 2010, doi: 10.1016/j.cell.2010.04.009.

[70] J. Geng, U. Nair, K. Yasumura-Yorimitsu, and D. J. Klionsky, "Post-Golgi Sec proteins are required for autophagy in Saccharomyces cerevisiae.," *Mol Biol Cell*, vol. 21, no. 13, pp. 2257–69, Jul. 2010, doi: 10.1091/mbc.e09-11-0969.

[71] C. Puri *et al.*, "The RAB11A-Positive Compartment Is a Primary Platform for Autophagosome Assembly Mediated by WIPI2 Recognition of PI3P-RAB11A.," *Dev Cell*, vol. 45, no. 1, pp. 114-131.e8, Apr. 2018, doi: 10.1016/j.devcel.2018.03.008.

[72] N. H. Patel, S. Bloukh, E. Alwohosh, A. Alhesa, T. Saleh, and D. A. Gewirtz, "Autophagy and senescence in cancer therapy," 2021, pp. 1–74. doi: 10.1016/bs.acr.2021.01.002.

[73] N. Gammoh and S. Wilkinson, "Autophagy in cancer biology and therapy," *Front Biol (Beijing)*, vol. 9, no. 1, pp. 35–50, Feb. 2014, doi: 10.1007/s11515-014-1294-2.

[74] Y.-K. Lee and J.-A. Lee, "Role of the mammalian ATG8/LC3 family in autophagy: differential and compensatory roles in the spatiotemporal regulation of autophagy.," *BMB Rep*, vol. 49, no. 8, pp. 424–30, Aug. 2016, doi: 10.5483/bmbrep.2016.49.8.081.

[75] N. Mizushima, "Autophagy: process and function.," *Genes Dev*, vol. 21, no. 22, pp. 2861–73, Nov. 2007, doi: 10.1101/gad.1599207.

[76] I. Tanida, T. Ueno, and E. Kominami, "LC3 and Autophagy.," *Methods Mol Biol*, vol. 445, pp. 77–88, 2008, doi: 10.1007/978-1-59745-157-4_4.

[77] D. A. Gewirtz, "The Four Faces of Autophagy: Implications for Cancer Therapy," *Cancer Res*, vol. 74, no. 3, pp. 647–651, Feb. 2014, doi: 10.1158/0008-5472.CAN-13-2966.

[78] D. A. Gewirtz, "Autophagy and senescence: a partnership in search of definition.," *Autophagy*, vol. 9, no. 5, pp. 808–12, May 2013, doi: 10.4161/auto.23922.

[79] C. Cao *et al.*, "Inhibition of Mammalian Target of Rapamycin or Apoptotic Pathway Induces Autophagy and Radiosensitizes PTEN Null Prostate Cancer Cells," *Cancer Res*, vol. 66, no. 20, pp. 10040–10047, Oct. 2006, doi: 10.1158/0008-5472.CAN-06-0802.

[80] K. Sharma, N. Le, M. Alotaibi, and D. Gewirtz, "Cytotoxic Autophagy in Cancer Therapy," *Int J Mol Sci*, vol. 15, no. 6, pp. 10034–10051, Jun. 2014, doi: 10.3390/ijms150610034.

[81] Q. Zhang *et al.*, "Berberine represses human gastric cancer cell growth in vitro and in vivo by inducing cytostatic autophagy via inhibition of MAPK/mTOR/p70S6K and Akt signaling pathways," *Biomedicine & Pharmacotherapy*, vol. 128, p. 110245, Aug. 2020, doi: 10.1016/j.biopha.2020.110245.

[82] C. H. Eng *et al.*, "Macroautophagy is dispensable for growth of KRAS mutant tumors and chloroquine efficacy," *Proceedings of the National Academy of Sciences*, vol. 113, no. 1, pp. 182–187, Jan. 2016, doi: 10.1073/pnas.1515617113.

[83] D. A. Gewirtz, "Cytoprotective and nonprotective autophagy in cancer therapy," *Autophagy*, vol. 9, no. 9, pp. 1263–1265, Sep. 2013, doi: 10.4161/auto.25233.

[84] J. Xu *et al.*, "Differential Radiation Sensitivity in p53 Wild-Type and p53-Deficient Tumor Cells Associated with Senescence but not Apoptosis or (Nonprotective) Autophagy," *Radiat Res*, vol. 190, no. 5, p. 538, Aug. 2018, doi: 10.1667/RR15099.1.

[85] T. Saleh, L. Tyutyunyk-Massey, N. H. Patel, E. K. Cudjoe, M. Alotaibi, and D. A. Gewirtz, "Studies of Non-Protective Autophagy Provide Evidence that Recovery from Therapy-Induced Senescence is Independent of Early Autophagy.," *Int J Mol Sci*, vol. 21, no. 4, Feb. 2020, doi: 10.3390/ijms21041427.

[86] O. Morana, W. Wood, and C. D. Gregory, "The Apoptosis Paradox in Cancer," *Int J Mol Sci*, vol. 23, no. 3, p. 1328, Jan. 2022, doi: 10.3390/ijms23031328.

[87] S. Goldar, M. S. Khaniani, S. M. Derakhshan, and B. Baradaran, "Molecular mechanisms of apoptosis and roles in cancer development and treatment.," *Asian Pac J Cancer Prev*, vol. 16, no. 6, pp. 2129–44, 2015, doi: 10.7314/apjcp.2015.16.6.2129.

[88] L. Ouyang *et al.*, "Programmed cell death pathways in cancer: a review of apoptosis, autophagy and programmed necrosis.," *Cell Prolif*, vol. 45, no. 6, pp. 487–98, Dec. 2012, doi: 10.1111/j.1365-2184.2012.00845.x.

[89]   S. Hassen, N. Ali, and P. Chowdhury, "Molecular signaling mechanisms of apoptosis in hereditary non-polyposis colorectal cancer.," *World J Gastrointest Pathophysiol*, vol. 3, no. 3, pp. 71–9, Jun. 2012, doi: 10.4291/wjgp.v3.i3.71.

[90]   Z. Jin and W. S. El-Deiry, "Overview of cell death signaling pathways.," *Cancer Biol Ther*, vol. 4, no. 2, pp. 139–63, Feb. 2005, doi: 10.4161/cbt.4.2.1508.

[91]   M. E. Guicciardi and G. J. Gores, "Life and death by death receptors.," *FASEB J*, vol. 23, no. 6, pp. 1625–37, Jun. 2009, doi: 10.1096/fj.08-111005.

[92]   P. Schneider and J. Tschopp, "Apoptosis induced by death receptors.," *Pharm Acta Helv*, vol. 74, no. 2–3, pp. 281–6, Mar. 2000, doi: 10.1016/s0031-6865(99)00038-2.

[93]   K. M. Boatright *et al.*, "A unified model for apical caspase activation.," *Mol Cell*, vol. 11, no. 2, pp. 529–41, Feb. 2003, doi: 10.1016/s1097-2765(03)00051-0.

[94]   S. Fulda, A. M. Gorman, O. Hori, and A. Samali, "Cellular stress responses: cell survival and cell death.," *Int J Cell Biol*, vol. 2010, p. 214074, 2010, doi: 10.1155/2010/214074.

[95]   D. Kashyap *et al.*, "Role of Reactive Oxygen Species in Cancer Progression," *Curr Pharmacol Rep*, vol. 5, no. 2, pp. 79–86, Apr. 2019, doi: 10.1007/s40495-019-00171-y.

[96]   C. Wang and R. J. Youle, "The role of mitochondria in apoptosis*.," *Annu Rev Genet*, vol. 43, pp. 95–118, 2009, doi: 10.1146/annurev-genet-102108-134850.

[97]   A. C. Belkina and G. V. Denis, "BET domain co-regulators in obesity, inflammation and cancer," *Nat Rev Cancer*, vol. 12, no. 7, pp. 465–477, Jul. 2012, doi: 10.1038/nrc3256.

[98]   B. Liu *et al.*, "BRD4-directed super-enhancer organization of transcription repression programs links to chemotherapeutic efficacy in breast cancer," *Proceedings of the National Academy of Sciences*, vol. 119, no. 6, Feb. 2022, doi: 10.1073/pnas.2109133119.

[99]   P. Filippakopoulos and S. Knapp, "Targeting bromodomains: epigenetic readers of lysine acetylation.," *Nat Rev Drug Discov*, vol. 13, no. 5, pp. 337–56, May 2014, doi: 10.1038/nrd4286.

[100]   K. L. Cheung *et al.*, "Distinct Roles of Brd2 and Brd4 in Potentiating the Transcriptional Program for Th17 Cell Differentiation.," *Mol Cell*, vol. 65, no. 6, pp. 1068-1080.e5, Mar. 2017, doi: 10.1016/j.molcel.2016.12.022.

[101]   M. Ba *et al.*, "BRD4 promotes gastric cancer progression through the transcriptional and epigenetic regulation of c-MYC.," *J Cell Biochem*, vol. 119, no. 1, pp. 973–982, Jan. 2018, doi: 10.1002/jcb.26264.

[102]   M. K. Jang, K. Mochizuki, M. Zhou, H.-S. Jeong, J. N. Brady, and K. Ozato, "The bromodomain protein Brd4 is a positive regulatory component of P-TEFb and stimulates RNA polymerase II-dependent transcription.," *Mol Cell*, vol. 19, no. 4, pp. 523–34, Aug. 2005, doi: 10.1016/j.molcel.2005.06.027.

[103]   B. Chapuy *et al.*, "Discovery and characterization of super-enhancer-associated dependencies in diffuse large B cell lymphoma.," *Cancer Cell*, vol. 24, no. 6, pp. 777–90, Dec. 2013, doi: 10.1016/j.ccr.2013.11.003.

[104]   M. S. Stratton *et al.*, "Signal-Dependent Recruitment of BRD4 to Cardiomyocyte Super-Enhancers Is Suppressed by a MicroRNA.," *Cell Rep*, vol. 16, no. 5, pp. 1366–1378, Aug. 2016, doi: 10.1016/j.celrep.2016.06.074.

[105]   C. A. French *et al.*, "BRD4 bromodomain gene rearrangement in aggressive carcinoma with translocation t(15;19).," *Am J Pathol*, vol. 159, no. 6, pp. 1987–92, Dec. 2001, doi: 10.1016/S0002-9440(10)63049-0.

[106] J. Zuber *et al.*, "RNAi screen identifies Brd4 as a therapeutic target in acute myeloid leukaemia." *Nature*, vol. 478, no. 7370, pp. 524–8, Aug. 2011, doi: 10.1038/nature10334.

[107] N. P. S. Crawford *et al.*, "Bromodomain 4 activation predicts breast cancer survival." *Proc Natl Acad Sci U S A*, vol. 105, no. 17, pp. 6380–5, Apr. 2008, doi: 10.1073/pnas.0710331105.

[108] J. E. Delmore *et al.*, "BET bromodomain inhibition as a therapeutic strategy to target c-Myc." *Cell*, vol. 146, no. 6, pp. 904–17, Sep. 2011, doi: 10.1016/j.cell.2011.08.017.

[109] S. Peirs *et al.*, "Targeting BET proteins improves the therapeutic efficacy of BCL-2 inhibition in T-cell acute lymphoblastic leukemia." *Leukemia*, vol. 31, no. 10, pp. 2037–2047, Oct. 2017, doi: 10.1038/leu.2017.10.

[110] P. Filippakopoulos *et al.*, "Selective inhibition of BET bromodomains." *Nature*, vol. 468, no. 7327, pp. 1067–73, Dec. 2010, doi: 10.1038/nature09504.

[111] T. Shimamura *et al.*, "Efficacy of BET bromodomain inhibition in Kras-mutant non-small cell lung cancer." *Clin Cancer Res*, vol. 19, no. 22, pp. 6183–92, Nov. 2013, doi: 10.1158/1078-0432.CCR-12-3904.

[112] J. Lu *et al.*, "Hijacking the E3 Ubiquitin Ligase Cereblon to Efficiently Target BRD4." *Chem Biol*, vol. 22, no. 6, pp. 755–63, Jun. 2015, doi: 10.1016/j.chembiol.2015.05.009.

[113] G. M. Burslem and C. M. Crews, "Proteolysis-Targeting Chimeras as Therapeutics and Tools for Biological Discovery." *Cell*, vol. 181, no. 1, pp. 102–114, Apr. 2020, doi: 10.1016/j.cell.2019.11.031.

[114] D. P. Bondeson *et al.*, "Catalytic in vivo protein knockdown by small-molecule PROTACs." *Nat Chem Biol*, vol. 11, no. 8, pp. 611–7, Aug. 2015, doi: 10.1038/nchembio.1858.

[115] F. Debacq-Chainiaux, J. D. Erusalimsky, J. Campisi, and O. Toussaint, "Protocols to detect senescence-associated beta-galactosidase (SA-βgal) activity, a biomarker of senescent cells in culture and in vivo," *Nat Protoc*, vol. 4, no. 12, pp. 1798–1806, Nov. 2009, doi: 10.1038/nprot.2009.191.

[116] G. F. Murray, D. Guest, A. Mikheykin, A. Toor, and J. Reed, "Single cell biomass tracking allows identification and isolation of rare targeted therapy-resistant DLBCL cells within a mixed population," *Analyst*, vol. 146, no. 4, pp. 1157–1162, Feb. 2021, doi: 10.1039/d0an01769h.

[117] D. Huang *et al.*, "High-Speed Live-Cell Interferometry: A New Method for Quantifying Tumor Drug Resistance and Heterogeneity," *Anal Chem*, vol. 90, no. 5, pp. 3299–3306, Mar. 2018, doi: 10.1021/acs.analchem.7b04828.

[118] Y. Makino *et al.*, "Comprehensive genomics in androgen receptor-dependent castration-resistant prostate cancer identifies an adaptation pathway mediated by opioid receptor kappa 1." *Commun Biol*, vol. 5, no. 1, p. 299, Apr. 2022, doi: 10.1038/s42003-022-03227-w.

[119] A. R. Lima *et al.*, "Discrimination between the human prostate normal and cancer cell exometabolome by GC-MS," *Sci Rep*, vol. 8, no. 1, p. 5539, Apr. 2018, doi: 10.1038/s41598-018-23847-9.

[120] N. Malaquin *et al.*, "DNA Damage- But Not Enzalutamide-Induced Senescence in Prostate Cancer Promotes Senolytic Bcl-xL Inhibitor Sensitivity," *Cells*, vol. 9, no. 7, Jul. 2020, doi: 10.3390/cells9071593.

[121] H. Vakifahmetoglu, M. Olsson, and B. Zhivotovsky, "Death through a tragedy: mitotic catastrophe.," *Cell Death Differ*, vol. 15, no. 7, pp. 1153–62, Jul. 2008, doi: 10.1038/cdd.2008.47.

[122] C. M. Beausejour, "Reversal of human cellular senescence: roles of the p53 and p16 pathways," *EMBO J*, vol. 22, no. 16, pp. 4212–4222, Aug. 2003, doi: 10.1093/emboj/cdg417.

[123] M. Narita *et al.*, "Rb-Mediated Heterochromatin Formation and Silencing of E2F Target Genes during Cellular Senescence," *Cell*, vol. 113, no. 6, pp. 703–716, Jun. 2003, doi: 10.1016/S0092-8674(03)00401-X.

[124] S. Pott and J. D. Lieb, "What are super-enhancers?," *Nat Genet*, vol. 47, no. 1, pp. 8–12, Jan. 2015, doi: 10.1038/ng.3167.

[125] N. M. Al Aboud, C. Tupper, and I. Jialal, "Genetics, Epigenetic Mechanism," *StatPearls*, Jan. 2023.

[126] Y. Jia, W.-J. Chng, and J. Zhou, "Super-enhancers: critical roles and therapeutic targets in hematologic malignancies.," *J Hematol Oncol*, vol. 12, no. 1, p. 77, Jul. 2019, doi: 10.1186/s13045-019-0757-y.

[127] G. A. Josling, S. A. Selvarajah, M. Petter, and M. F. Duffy, "The role of bromodomain proteins in regulating gene expression.," *Genes (Basel)*, vol. 3, no. 2, pp. 320–43, May 2012, doi: 10.3390/genes3020320.

[128] Y. Sun, J. Han, Z. Wang, X. Li, Y. Sun, and Z. Hu, "Safety and Efficacy of Bromodomain and Extra-Terminal Inhibitors for the Treatment of Hematological Malignancies and Solid Tumors: A Systematic Study of Clinical Trials," *Front Pharmacol*, vol. 11, Jan. 2021, doi: 10.3389/fphar.2020.621093.

[129] P. Filippakopoulos *et al.*, "Selective inhibition of BET bromodomains," *Nature*, vol. 468, no. 7327, pp. 1067–1073, Dec. 2010, doi: 10.1038/nature09504.

[130] P. Filippakopoulos *et al.*, "Histone Recognition and Large-Scale Structural Analysis of the Human Bromodomain Family," *Cell*, vol. 149, no. 1, pp. 214–231, Mar. 2012, doi: 10.1016/j.cell.2012.02.013.

[131] S. A. Piha-Paul *et al.*, "First-in-Human Study of Mivebresib (ABBV-075), an Oral Pan-Inhibitor of Bromodomain and Extra Terminal Proteins, in Patients with Relapsed/Refractory Solid Tumors.," *Clin Cancer Res*, vol. 25, no. 21, pp. 6309–6319, Nov. 2019, doi: 10.1158/1078-0432.CCR-19-0578.

[132] X. Liao *et al.*, "ARV-825 Demonstrates Antitumor Activity in Gastric Cancer via MYC-Targets and G2M-Checkpoint Signaling Pathways.," *Front Oncol*, vol. 11, p. 753119, 2021, doi: 10.3389/fonc.2021.753119.

[133] M. Wakita *et al.*, "A BET family protein degrader provokes senolysis by targeting NHEJ and autophagy in senescent cells," *Nat Commun*, vol. 11, no. 1, p. 1935, Apr. 2020, doi: 10.1038/s41467-020-15719-6.

[134] N. H. Patel, J. Xu, T. Saleh, Y. Wu, S. Lima, and D. A. Gewirtz, "Influence of nonprotective autophagy and the autophagic switch on sensitivity to cisplatin in non-small cell lung cancer cells.," *Biochem Pharmacol*, vol. 175, p. 113896, May 2020, doi: 10.1016/j.bcp.2020.113896.

[135] F. Ahmadinejad *et al.*, "Senolytic-Mediated Elimination of Head and Neck Tumor Cells Induced Into Senescence by Cisplatin.," *Mol Pharmacol*, vol. 101, no. 3, pp. 168–180, Mar. 2022, doi: 10.1124/molpharm.121.000354.

[136] R. M. Finnegan *et al.*, "The BET inhibitor/degrader ARV-825 prolongs the growth arrest response to Fulvestrant + Palbociclib and suppresses proliferative recovery in ER-positive breast cancer," *Front Oncol*, vol. 12, Jan. 2023, doi: 10.3389/fonc.2022.966441.

[137] H. Soylu, M. Kırca, S. Avcı, B. Ozpolat, and I. Ustunel, "Antiandrogen abiraterone and docetaxel treatments affect Notch1, Jagged1 and Hes1 expressions in metastatic prostate cancer cells," *Exp Mol Pathol*, vol. 119, p. 104607, Apr. 2021, doi: 10.1016/j.yexmp.2021.104607.

[138] M. Barrado *et al.*, "Radiopotentiation of enzalutamide over human prostate cancer cells as assessed by real-time cell monitoring," *Reports of Practical Oncology & Radiotherapy*, vol. 24, no. 2, pp. 221–226, Mar. 2019, doi: 10.1016/j.rpor.2019.02.002.

[139] K. E. Ware *et al.*, "Snail promotes resistance to enzalutamide through regulation of androgen receptor activity in prostate cancer," *Oncotarget*, vol. 7, no. 31, pp. 50507–50521, Aug. 2016, doi: 10.18632/oncotarget.10476.

[140] F. Alimirah, J. Chen, Z. Basrawala, H. Xin, and D. Choubey, "DU-145 and PC-3 human prostate cancer cell lines express androgen receptor: Implications for the androgen receptor functions and regulation," *FEBS Lett*, vol. 580, no. 9, pp. 2294–2300, Apr. 2006, doi: 10.1016/j.febslet.2006.03.041.

[141] J. A. Gibbons *et al.*, "Clinical Pharmacokinetic Studies of Enzalutamide.," *Clin Pharmacokinet*, vol. 54, no. 10, pp. 1043–55, Oct. 2015, doi: 10.1007/s40262-015-0271-5.

[142] Y. Rehman and J. E. Rosenberg, "Abiraterone acetate: oral androgen biosynthesis inhibitor for treatment of castration-resistant prostate cancer.," *Drug Des Devel Ther*, vol. 6, pp. 13–8, 2012, doi: 10.2147/DDDT.S15850.

[143] F. Saad, "Evidence for the efficacy of enzalutamide in postchemotherapy metastatic castrate-resistant prostate cancer.," *Ther Adv Urol*, vol. 5, no. 4, pp. 201–10, Aug. 2013, doi: 10.1177/1756287213490054.

[144] H. G. Nguyen *et al.*, "Targeting autophagy overcomes Enzalutamide resistance in castration-resistant prostate cancer cells and improves therapeutic response in a xenograft model," *Oncogene*, vol. 33, no. 36, pp. 4521–4530, Sep. 2014, doi: 10.1038/onc.2014.25.

[145] M. P. Thomé *et al.*, "Ratiometric analysis of acridine orange staining in the study of acidic organelles and autophagy," *J Cell Sci*, Jan. 2016, doi: 10.1242/jcs.195057.

[146] A. M. Schläfli *et al.*, "Prognostic value of the autophagy markers LC3 and p62/SQSTM1 in early-stage non-small cell lung cancer.," *Oncotarget*, vol. 7, no. 26, pp. 39544–39555, Jun. 2016, doi: 10.18632/oncotarget.9647.

[147] Y. Kabeya *et al.*, "LC3, a mammalian homologue of yeast Apg8p, is localized in autophagosome membranes after processing.," *EMBO J*, vol. 19, no. 21, pp. 5720–8, Nov. 2000, doi: 10.1093/emboj/19.21.5720.

[148] Y. Kabeya, N. Mizushima, A. Yamamoto, S. Oshitani-Okamoto, Y. Ohsumi, and T. Yoshimori, "LC3, GABARAP and GATE16 localize to autophagosomal membrane depending on form-II formation.," *J Cell Sci*, vol. 117, no. Pt 13, pp. 2805–12, Jun. 2004, doi: 10.1242/jcs.01131.

[149] N. Mizushima and T. Yoshimori, "How to Interpret LC3 Immunoblotting," *Autophagy*, vol. 3, no. 6, pp. 542–545, Nov. 2007, doi: 10.4161/auto.4600.

[150] Y. Tan *et al.*, "Inhibition of BRD4 suppresses tumor growth in prostate cancer via the enhancement of FOXO1 expression." *Int J Oncol*, vol. 53, no. 6, pp. 2503–2517, Dec. 2018, doi: 10.3892/ijo.2018.4577.

[151] H. Wang, M. Guo, H. Wei, and Y. Chen, "Targeting MCL-1 in cancer: current status and perspectives," *J Hematol Oncol*, vol. 14, no. 1, p. 67, Apr. 2021, doi: 10.1186/s13045-021-01079-1.

[152] H. Widden and W. J. Placzek, "The multiple mechanisms of MCL1 in the regulation of cell fate," *Commun Biol*, vol. 4, no. 1, p. 1029, Sep. 2021, doi: 10.1038/s42003-021-02564-6.

[153] E. Bolesta *et al.*, "Inhibition of Mcl-1 promotes senescence in cancer cells: implications for preventing tumor growth and chemotherapy resistance." *Mol Cell Biol*, vol. 32, no. 10, pp. 1879–92, May 2012, doi: 10.1128/MCB.06214-11.

[154] P. L. Palmbos *et al.*, "A Randomized Phase II Study of Androgen Deprivation Therapy with or without Palbociclib in RB-positive Metastatic Hormone-Sensitive Prostate Cancer," *Clinical Cancer Research*, vol. 27, no. 11, pp. 3017–3027, Jun. 2021, doi: 10.1158/1078-0432.CCR-21-0024.

[155] C. L. Braal, E. M. Jongbloed, S. M. Wilting, R. H. J. Mathijssen, S. L. W. Koolen, and A. Jager, "Inhibiting CDK4/6 in Breast Cancer with Palbociclib, Ribociclib, and Abemaciclib: Similarities and Differences." *Drugs*, vol. 81, no. 3, pp. 317–331, Feb. 2021, doi: 10.1007/s40265-020-01461-2.

[156] B. R. Topacio *et al.*, "Cyclin D-Cdk4,6 Drives Cell-Cycle Progression via the Retinoblastoma Protein's C-Terminal Helix." *Mol Cell*, vol. 74, no. 4, pp. 758-770.e4, May 2019, doi: 10.1016/j.molcel.2019.03.020.

[157] M. Troiani *et al.*, "Single-cell transcriptomics identifies Mcl-1 as a target for senolytic therapy in cancer." *Nat Commun*, vol. 13, no. 1, p. 2177, Apr. 2022, doi: 10.1038/s41467-022-29824-1.

[158] S. D. Baker, A. Sparreboom, and J. Verweij, "Clinical Pharmacokinetics of Docetaxel," *Clin Pharmacokinet*, vol. 45, no. 3, pp. 235–252, 2006, doi: 10.2165/00003088-200645030-00002.

[159] S. K. Madden, A. D. de Araujo, M. Gerhardt, D. P. Fairlie, and J. M. Mason, "Taking the Myc out of cancer: toward therapeutic strategies to directly inhibit c-Myc," *Mol Cancer*, vol. 20, no. 1, p. 3, Jan. 2021, doi: 10.1186/s12943-020-01291-6.

[160] A. Höhn *et al.*, "Happily (n)ever after: Aging in the context of oxidative stress, proteostasis loss and cellular senescence," *Redox Biol*, vol. 11, pp. 482–501, Apr. 2017, doi: 10.1016/j.redox.2016.12.001.

[161] K. R. Parzych and D. J. Klionsky, "An overview of autophagy: morphology, mechanism, and regulation." *Antioxid Redox Signal*, vol. 20, no. 3, pp. 460–73, Jan. 2014, doi: 10.1089/ars.2013.5371.

[162] D. Kashyap, V. K. Garg, and N. Goel, "Intrinsic and extrinsic pathways of apoptosis: Role in cancer development and prognosis," 2021, pp. 73–120. doi: 10.1016/bs.apcsb.2021.01.003.